JOURNAL OF GUIDANCE, CONTROL, AND DYNAMICS
Vol. 28, No. 5, September–October 2005

Fault-Tolerant Robust Automatic Landing Control Design

Fang Liao*
National University of Singapore, Singapore 117508, Republic of Singapore
Jian Liang Wang†
Nanyang Technological University, Singapore 639798, Republic of Singapore
and
Eng Kee Poh‡ and Dong Li§
DSO National Laboratories, Singapore 118230, Republic of Singapore

A new approach is presented for developing reliable automatic landing controllers that can tolerate actuator stuck faults. The approach is based on the solvability of linear matrix inequalities and polytopic fault models. The H_2 control technique is used to guarantee tracking performance with respect to a given glide slope trajectory. A high-fidelity fighter aircraft model is studied to illustrate the proposed approach. The six-degree-of-freedom nonlinear aircraft model with independent left and right control surfaces is established using the appropriate aerodynamic data from wind-tunnel test and computational fluid dynamics. A single fixed reliable automatic landing controller is designed for the whole landing process. It achieves optimized tracking performance in normal operation and maintains an acceptable level of tracking performance in the case of single contingency actuator stuck fault among the left and right ailerons and horizontal stabilators. Nonlinear simulation under various faults, measurement noises, and wind disturbances such as deterministic wind, wind turbulence, and wind shear are included in this study. Simulation results show that such a reliable controller design approach can achieve zero steady-state tracking error, good tracking response, robustness against wind disturbances, and reliability against actuator stuck faults.

Nomenclature

b	=	wing span, m
$C_{m,t}$, $C_{n,t}$, $C_{l,t}$	=	total pitching, yawing, and rolling-moment coefficient
$C_{x,t}$, $C_{y,t}$, $C_{z,t}$	=	total X-, Y-, and Z-axis force coefficients
$\bar{c}$	=	wing mean aerodynamic chord, m
d_{lat}	=	lateral error from glideslope centerline, m
d_{lon}	=	longitudinal error from glideslope centerline, m
g	=	acceleration caused by gravity, $= 9.81$ m/s^2
H_e	=	engine angular momentum, kg-m^2/s
h	=	altitude, m
I_x, I_y, I_z	=	moment of inertia about X, Y, and Z body axes, kg-m^2
I_{xz}	=	product of inertia with respect to X and Z body axes, kg-m^2
m	=	aircraft mass, kg
P_E	=	eastward distance, m
p	=	aircraft roll rate about X body axis, rad/s
p_s, $\bar{q}$	=	static pressure and freestream dynamic pressure, N/m^2
q	=	aircraft pitch rate about Y body axis, rad/s
r	=	aircraft yaw rate about Z body axis, rad/s
S	=	wing area, m^2
T	=	engine thrust, N
u, v, w	=	components of aircraft velocity along X, Y, and Z body axes, m/s
V_t	=	aircraft resultant airspeed, m/s
W_{bx}, W_{by}, W_{bz}	=	components of wind disturbance along X, Y, and Z body axes, m/s
X_{cg}	=	center of gravity, fraction of $\bar{c}$
α	=	angle of attack, deg
β	=	angle of sideslip, deg
Γ	=	glide slope angle, deg
δ_{al}	=	left aileron deflection, positive for downward, deg
δ_{ar}	=	right aileron deflection, positive for downward, deg
δ_{hl}	=	left horizontal stabilator deflection, positive for downward, deg
δ_{hr}	=	right horizontal stabilator deflection, positive for downward, deg
δ_r	=	rudder deflection, positive for leftward, deg
δ_T	=	engine throttle, %
θ	=	pitch angle, deg
ρ	=	atmosphere density, kg/m^3
ϕ	=	roll angle, deg
ψ	=	yaw angle, deg

Received 3 August 2004; presented as Paper 2004-5233 at the AIAA Guidance, Navigation, and Control Conference, Providence, RI, 16–19 August 2004; revision received 18 November 2004; accepted for publication 18 November 2004.

*Research Scientist, Temasek Laboratories, 5 Sports Drive 2; tsllf@nus.edu.sg.
†Associate Professor, School of Electrical and Electronic Engineering, Nanyang Avenue.
‡Principal Member of Technical Staff, Unmanned System Center, 20 Science Park Drive. Member AIAA.
§Senior Member of Technical Staff, Unmanned System Center, 20 Science Park Drive.

I. Introduction

AS is well known, landing is the most challenging among all aircraft flight phases. During landing, aircraft flies at a considerable low altitude and low speed, and hence accidents are more likely to happen. Many uncertain factors, such as wind turbulence and wind shear, become critical because of low altitude and low speed. Measurement noise in the feedback signal is also stronger at ground level. Naturally, robustness to these uncertainties is a main challenge in the design of standard autolanding systems. During landing, aircraft must track a desired trajectory satisfying Federal Aviation Administration (FAA) requirements[1] until it arrives at the

touchdown point on the runway. Therefore, tracking performance is actually another main challenge in the design of autolanding systems. There are many methods to design the autolanding control law.[2–7] Shue and Agarwal[2] have developed a mixed H_2/H_∞ control technique for the design of autolanding systems. Ochi and Kanai[4] adopted H_∞ control to design automatic approach and landing for propulsion-controlled aircraft. But the robustness of controller in the presence of wind shear was not addressed, and neither was accurate tracking performance. Neural networks were also used in the design of autolanding systems by Miller et al.[5] and Sanai and Balakrishnan.[6] However, the neural-network approach is only effective within the special training set. A common weakness of these approaches is that they do not control the aircraft to track the desired flight path accurately. Recently, Che and Chen[7] presented an autolanding control law to achieve both robustness and accurate tracking by combining robust H_∞ control and stable inversion. However, only the longitudinal control was studied, and the calculation of the stable inversion was off-line based on the desired landing trajectory.

During the landing process, besides uncertainties and disturbances, faults can unexpectedly occur. Hence in addition to tracking accuracy and robustness against uncertainties and disturbances, reliability against faults is also a major challenge in the design of autolanding systems. Reliable control/fault-tolerant control has been studied by many authors (see Refs. 8–13 and the reference therein), and several approaches have been proposed to design reliable controllers against actuator stuck faults. An adaptive control scheme was presented to deal with actuator stuck faults in Refs. 10 and 11. However, it is only suitable for systems with modular-redundant actuators. In Ref. 12, a stuck fault was modeled as a bounded input, and its effect on the closed-loop system was described by a peak-to-peak gain. Nevertheless, this approach is not always efficient in practice because an iterative algorithm that achieves at most local optimum and can have convergence problems is involved. Although automatic landing control and reliable control methods have been extensively studied, to the best knowledge of the authors, so far few papers are devoted to reliable automatic landing control.

In this paper, a reliable robust H_2 integral control approach is presented to design a single fixed controller that performs well during the whole landing process from wing-level flight to flare. The designed controller cannot only reject wind disturbances but also tolerate actuator stuck faults. Moreover, it achieves tracking accuracy of category III specification.[1] This approach is based on linear matrix inequalities (LMIs) and polytopic fault models. It optimizes closed-loop system tracking performance in normal operation under the constraints of tracking performance bounds in the event of faults.

The rest of the paper is organized as follows. The aircraft models under the normal and faulty operations are presented in Sec. II, together with models for deterministic wind, wind turbulence, and wind shear. The reliable automatic landing problem is formulated in Sec. III, and the reliable robust H_2 autolanding controller is designed in Sec. IV. Section V gives the results of nonlinear simulation studies, followed by some concluding remarks in Sec. VI.

II. Aircraft Model and Wind Models

A. Nonlinear Aircraft Model

In this study, a high-fidelity fighter aircraft model is used to demonstrate the proposed reliable autolanding control approach. The dynamics of the aircraft are highly nonlinear. Under the rigid-body assumption, the six-degree-of-freedom equations of motion, referenced to a body-fixed axis system, are given as follows.

Forces equations:

$$\dot{u} = rv - qw - g\sin\theta + (\bar{q}S/m)C_{X,t} + T/m \tag{1}$$

$$\dot{v} = pw - ru + g\cos\theta\sin\phi + (\bar{q}S/m)C_{Y,t} \tag{2}$$

$$\dot{w} = qu - pv + g\cos\theta\cos\phi + (\bar{q}S/m)C_{Z,t} \tag{3}$$

Moment equations:

$$\dot{p} = \frac{I_Y - I_Z}{I_X}qr + \frac{I_{XZ}}{I_X}(\dot{r} + pq) + \frac{\bar{q}Sb}{I_X}C_{l,t} \tag{4}$$

$$\dot{q} = \frac{I_Z - I_X}{I_Y}pr + \frac{I_{XZ}}{I_Y}(r^2 - p^2) + \frac{\bar{q}S\bar{c}}{I_Y}C_{m,t} - \frac{H_e}{I_Y}r \tag{5}$$

$$\dot{r} = \frac{I_X - I_Y}{I_Z}pq + \frac{I_{XZ}}{I_Z}(\dot{p} - qr) + \frac{\bar{q}Sb}{I_Z}C_{n,t} + \frac{H_e}{I_Z}q \tag{6}$$

$C_{X,t}$, $C_{Y,t}$, and $C_{Z,t}$ and $C_{l,t}$, $C_{m,t}$, and $C_{n,t}$ are functions of deflection of control surfaces such as δ_{al}, δ_{ar}, δ_{hl}, δ_{hr}, and δ_r (see Refs. 14 and 15 for details).

Auxiliary equations include the following.

Angle of attack:

$$\alpha = \tan^{-1}(w/u) \tag{7}$$

Sideslip angle:

$$\beta = \sin^{-1}(v/V_t) \tag{8}$$

Resultant airspeed:

$$V_t = \sqrt{u^2 + v^2 + w^2} \tag{9}$$

The leading-edge flap deflection δ_{lef} is scheduled with α and $\bar{q}/p_s$ as follows:

$$\delta_{\text{lef}} = 1.38\frac{2S + 7.25}{S + 7.25}\alpha - 9.05\frac{\bar{q}}{p_s} + 1.45 \tag{10}$$

B. Actuator Dynamics

The horizontal stabilator actuators are modeled as first-order lags of 0.0495 s with rate limits of ±60 deg/s and deflection limits of ±25 deg. The aileron actuators are modeled as first-order lags of 0.0495 s with rate limits of ±80 deg/s and deflection limits of ±20 deg. The rudder actuator is modeled as a first-order lag of 0.0495 s with rate limits of ±120 deg/s and deflection limits of ±30 deg.

C. Wind Model

In this paper, several types of wind disturbances, such as deterministic wind, wind turbulence, and wind shear, are considered in the landing process. Their mathematic models are given as follows.

1. *Deterministic Wind*

Consider the International Civil Aviation Organization standard atmosphere. A typical idealized wind profile is given by

$$V_w = \begin{cases} 0, & h > 470 \text{ m} \\ 2.86585V_{w9.15}, & 300 \text{ m} < h \le 470 \text{ m} \\ V_{w9.15}\dfrac{h^{0.2545} - 0.4097}{1.3470}, & 0 < h \le 300 \text{ m} \end{cases} \tag{11}$$

where $V_{w9.15}$ is the wind speed at 9.15 m altitude. The wind profile is shown in Fig. 1.

2. *Wind Turbulence*

In this study, a Dryden spectrum is used to model wind turbulence. Mathematically, it is represented by

$$u_g = u_{g1} + u_{\text{gc}} \tag{12}$$

$$\dot{u}_{g1} = 0.2|u_{\text{gc}}|\sqrt{2a_u}\,N_1 - a_u u_{g1} \tag{13}$$

where u_{g1} is the turbulence component, u_{gc} is the mean wind with

$$u_{\text{gc}} = \begin{cases} -u_0\left(1 + \ell_n\dfrac{h}{510}\Big/\ell_n 51\right), & h \ge 10 \text{ ft} \\ 0, & h < 10 \text{ ft} \end{cases} \tag{14}$$

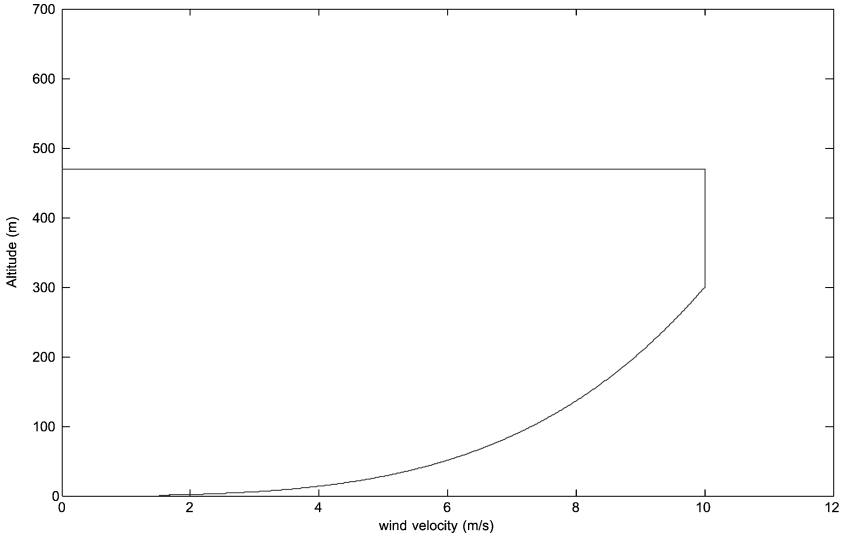

Fig. 1 Profile of deterministic wind.

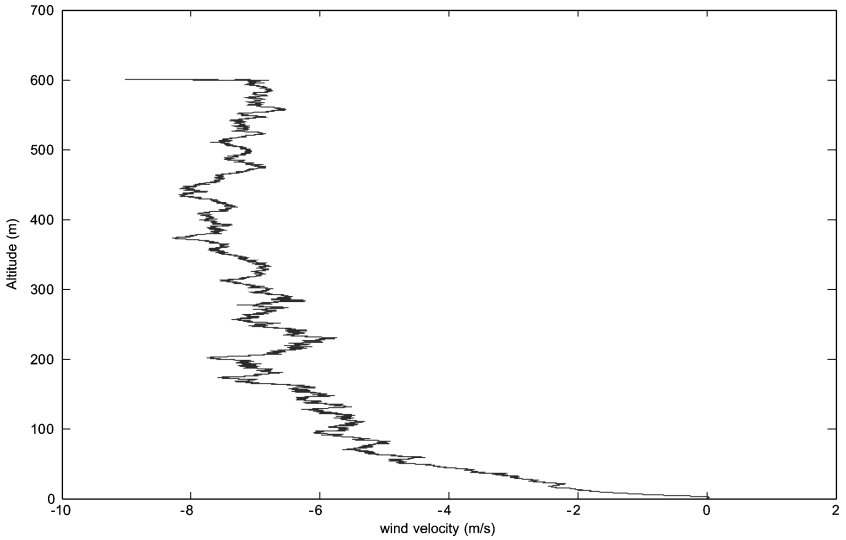

Fig. 2 Turbulence profile.

where u_0 is 20 ft/s, N_1 is the Gaussian random noises with zero mean and variance 100, and

$$a_u = \begin{cases} V_0 \Big/ \left(100 \sqrt[3]{h}\right), & h > 230 \text{ ft} \\ V_0/600, & h \le 230 \text{ ft} \end{cases} \tag{15}$$

with V_0 referring to the trimmed aircraft speed. The units used here are feet and feet/second.

The profile of wind turbulence plotted in meters and meters/second is given in Fig. 2.

3. Wind-Shear Model

At a given height h_{shear}, a wind shear in vertical direction (microburst) is generated by suddenly changing the direction of the vertical wind from up to down, that is,

$$w_{\text{gc}} = \begin{cases} 0, & h > 510 \text{ ft} \\ -w_0 \left(1 + \ell_n \dfrac{h}{510} \Big/ \ell_n 51\right), & 0 < h \le 510 \text{ ft} \end{cases} \tag{16}$$

where w_0 is 40 ft/s above the height of h_{shear} and -40 ft/s under h_{shear}. Here h_{shear} is 300 ft. Although 40 ft/s is not as severe as recorded in Ref. 16, it is big enough to model most common microburst produced by a thunderstorm. Figure 3 gives the curve of wind velocity (in meters/second) vs altitude (in meters).

D. Linear Aircraft Fault Model

Using the small-perturbation assumption from the steady-state condition, a set of linear constant-coefficient state equations can be derived. Usually, an aircraft with independent control surfaces has at least five independent control surfaces, that is, the left horizontal stabilator δ_{hl}, the right horizontal stabilator δ_{hr}, the left aileron δ_{al}, the right aileron δ_{ar}, and the rudder δ_r. Aircraft actuator stuck faults can happen in any one or more of these control surfaces. To tolerate such faults, a set of stuck faults can be selected as design vertices. Each vertex fault model can be obtained by linearizing the aircraft model when the corresponding vertex fault occurs. For design purposes, the aircraft model (with or without such faults) is assumed to be modeled by a polytopic fault system, whose vertices consist of normal aircraft model and the just-selected vertex fault models. Intermediate faults between those vertices are assumed to be within the polytope, hence covered by the polytopic fault model. If this is not the case, then more vertex faults and vertex fault models can be considered in the design. Therefore, polytopic fault systems can be used to model an aircraft with actuator stuck faults.

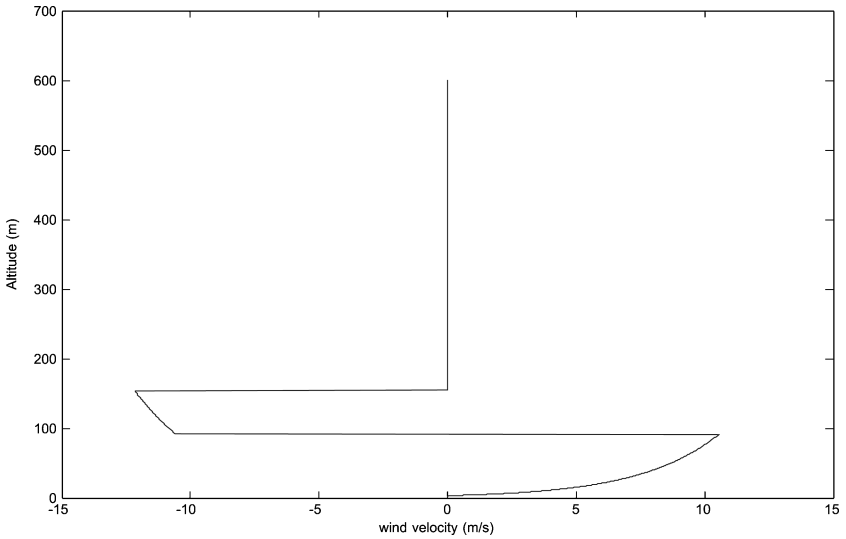

Fig. 3 Wind-shear profile.

In this paper, we adopt the polytopic fault model of the form

$$\dot{\boldsymbol{x}}_p = \boldsymbol{A}_p(\Theta)\boldsymbol{x}_p + \boldsymbol{B}_p(\Theta)\boldsymbol{u} + \boldsymbol{G}_p(\Theta)\boldsymbol{w}, \qquad \boldsymbol{y} = \boldsymbol{C}_p(\Theta)\boldsymbol{x}_p \quad (17)$$

where $\boldsymbol{x}_p \in \boldsymbol{R}^n$ is the state vector and $\boldsymbol{x}_p = [u\ \ w\ \ q\ \ \theta\ \ v\ \ p\ \ r\ \ \phi\ \ \psi\ \ P_E]^T$; $\boldsymbol{y} \in \boldsymbol{R}^p$ is the measurement output vector and $\boldsymbol{y} = [\beta\ \ \dot{h}\ \ d_{\text{lat}}]^T$; $\boldsymbol{u} \in \boldsymbol{R}^m$ is the control input vector and $\boldsymbol{u} = [\delta_{\text{hl}}\ \ \delta_{\text{hr}}\ \ \delta_{\text{al}}\ \ \delta_{\text{ar}}\ \ \delta_r]^T$; $\boldsymbol{w} \in \boldsymbol{R}^h$ is the disturbance vector and $\boldsymbol{w} = [W_{bx}\ \ W_{by}\ \ W_{bz}]^T$. The uncertain parameter $\Theta = [\theta_0\ \ \theta_1\ \ \cdots\ \ \theta_l]^T \in \boldsymbol{R}^{l+1}$ satisfies

$$\Theta \in \boldsymbol{\Theta} \triangleq \left\{ \Theta \in \boldsymbol{R}^{l+1} : \theta_i \geq 0, \qquad \sum_{i=0}^{l} \theta_i = 1 \right\} \quad (18)$$

The system matrices are parameterized as

$$\boldsymbol{A}_p(\Theta) = \sum_{i=0}^{l} \boldsymbol{A}_{\text{pi}}\theta_i, \qquad \boldsymbol{B}_p(\Theta) = \sum_{i=0}^{l} \boldsymbol{B}_{\text{pi}}\theta_i$$

$$\boldsymbol{G}_p(\Theta) = \sum_{i=0}^{l} \boldsymbol{G}_{\text{pi}}\theta_i, \qquad \boldsymbol{C}_p(\Theta) = \sum_{i=0}^{l} \boldsymbol{C}_{\text{pi}}\theta_i \quad (19)$$

where $(\boldsymbol{A}_{\text{pi}}, \boldsymbol{B}_{\text{pi}}, \boldsymbol{C}_{\text{pi}}, \boldsymbol{G}_{\text{pi}})$ $(i = 0, 1, \ldots, l)$ are known constant matrices of appropriate dimensions that represent the vertices of possible fault models. Among these vertices, one corresponds to the normal case (no fault), and the remaining l correspond to the fault cases. Without loss of generality, suppose that $i = 0$, that is, $(\boldsymbol{A}_{p0}, \boldsymbol{B}_{p0}, \boldsymbol{C}_{p0}, \boldsymbol{G}_{p0})$, corresponds to the normal case. The parameter Θ provides the interpolation between the vertices.

In this study, the normal aircraft is trimmed for wing-level flight, where its steady-state equilibrium conditions are as follows:

$$\delta_{\text{hl}} = -1.6077 \text{ deg}, \qquad \delta_{\text{hr}} = -1.6077 \text{ deg}, \qquad \psi = 0 \text{ deg}$$

$$p = 0.0, \qquad \delta_{\text{al}} = 0.0 \text{ deg}, \qquad \delta_{\text{ar}} = 0.0 \text{ deg}, \qquad \theta = 11.0 \text{ deg}$$

$$q = 0.0, \qquad \delta_r = 0.0 \text{ deg}, \qquad \delta_T = 0.1871, \qquad \phi = 0.0 \text{ deg}$$

$$r = 0.0, \qquad X_{\text{cg}} = 0.35\bar{c}, \qquad \alpha = 11.0 \text{ deg}$$

$$V_t = 82.88 \text{ m/s}, \qquad \beta = 0.0 \text{ deg}, \qquad h = 600 \text{ m}$$

Consider the following 6 $(l = 6)$ single contingency vertex faults:

1) The left aileron δ_{al} is stuck at $+20$ deg with linear model $(\boldsymbol{A}_{p1}, \boldsymbol{B}_{p1}, \boldsymbol{C}_{p1}, \boldsymbol{G}_{p1})$.

2) The left aileron δ_{al} is stuck at -20 deg with linear model $(\boldsymbol{A}_{p2}, \boldsymbol{B}_{p2}, \boldsymbol{C}_{p2}, \boldsymbol{G}_{p2})$.

3) The right aileron δ_{ar} is stuck at $+20$ deg with linear model $(\boldsymbol{A}_{p3}, \boldsymbol{B}_{p3}, \boldsymbol{C}_{p3}, \boldsymbol{G}_{p3})$.

4) The right aileron δ_{ar} is stuck at -20 deg with linear model $(\boldsymbol{A}_{p4}, \boldsymbol{B}_{p4}, \boldsymbol{C}_{p4}, \boldsymbol{G}_{p4})$.

5) The left horizontal stabilator δ_{hl} is stuck at 0 deg with linear model $(\boldsymbol{A}_{p5}, \boldsymbol{B}_{p5}, \boldsymbol{C}_{p5}, \boldsymbol{G}_{p5})$.

6) The right horizontal stabilator δ_{hr} is stuck at 0 deg with linear model $(\boldsymbol{A}_{p6}, \boldsymbol{B}_{p6}, \boldsymbol{C}_{p6}, \boldsymbol{G}_{p6})$.

The linearized system matrices $(\boldsymbol{A}_{\text{pi}}, \boldsymbol{B}_{\text{pi}}, \boldsymbol{C}_{\text{pi}}, \boldsymbol{G}_{\text{pi}})$ $(i = 0, 1, \ldots, 6)$ are given in the Appendix. As the preceding vertex fault models are obtained by linearizing the aircraft model with only one of the actuators being stuck, the corresponding polytopic fault system describes single contingency actuator stuck fault. That is, at each time, only one of the actuators can be stuck. The following fault cases can be covered by the polytopic fault system:

1) The left aileron δ_{al} is stuck from -20 to $+20$ deg.

2) The right aileron δ_{al} is stuck from -20 to $+20$ deg.

3) The left horizontal stabilator δ_{hl} is stuck at 0 deg.

4) The right horizontal stabilator δ_{hl} is stuck at 0 deg.

Note that there is a certain degree of overdesign in adopting the polytopic fault model as the interpolation among some of the vertices might not correspond to any physical reality. For example, the interpolation between the model for δ_{al} stuck at 20 deg and the model for δ_{ar} stuck at 20 deg might not have much physical meaning. However, this overdesign will ensure that the designed performance can be achieved when there are model uncertainties in the vertex models and discrepancies/inaccuracies in the interpolated intermediate-fault models.

III. Problem Formulation of Reliable Automatic Landing

Define the tracking error vector $\boldsymbol{e}$ as

$$\boldsymbol{e} = \boldsymbol{r} - \boldsymbol{y} \quad (20)$$

where $\boldsymbol{r} \in \boldsymbol{R}^p$ is the reference signal vector and $\boldsymbol{y} \in \boldsymbol{R}^p$ is the measurement output vector. During the automatic landing process, the aircraft is required to track the glide path centerline and keep its angle of sideslip at zero. One of feasible control solutions is to ensure that the angle of sideslip β and lateral error d_{lat} signal track zero step commands, and the altitude signal tracks a known altitude command profile consisting of step, ramp, and exponential commands. To

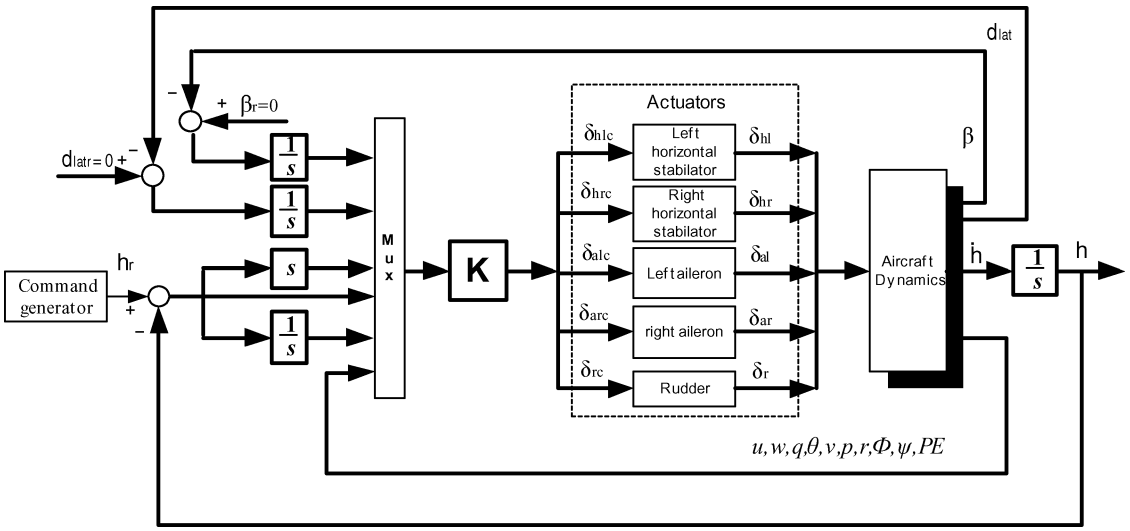

Fig. 4 Block diagram of automatic landing control system.

improve system performance, proportional, integral, derivative (PID) control of altitude is adopted, and integral signals of tracking errors are introduced to eliminate steady-state tracking errors. In the robust controller design, the derivative of tracking error of altitude can be described as

$$\dot{e}_h(t) = \dot{h}_r(t) - \dot{h}(t) \approx [\mu/(s+\mu)][\dot{h}_r(t) - \dot{h}(t)] \tag{21}$$

where h_r is the altitude command profile, s is Laplace variable, and $\mu > 0$ is a sufficiently large scalar. For $\mu \gg 1$, Eq. (21) can be written in the form of state space as

$$\ddot{e}_h(t) = -\mu\dot{e}_h(t) + \mu[\dot{h}_r(t) - \dot{h}(t)] \tag{22}$$

After introducing the tracking error integral signals of the sideslip angle β and the lateral error d_{lat} and PID signals of the altitude h, an augmented state-space system model of system (17) is given by

$$\dot{\boldsymbol{x}}_a = \boldsymbol{A}_a(\Theta)\boldsymbol{x}_a + \boldsymbol{B}_a(\Theta)\boldsymbol{u} + \boldsymbol{G}(\Theta)\boldsymbol{w}_a, \qquad \boldsymbol{z} = \boldsymbol{C}_1\boldsymbol{x}_a + \boldsymbol{D}_1\boldsymbol{u} \tag{23}$$

Here the augmented state vector is defined as

$$\boldsymbol{x}_a = \left[\int_0^t e_\beta \,\mathrm{d}t \quad \dot{e}_h \quad \int_0^t e_{\text{lat}}\,\mathrm{d}t \quad e_h \quad \int_0^t e_h\,\mathrm{d}t \quad \boldsymbol{x}_p^T\right]^T$$

with e_β, e_h, and e_{lat} being the sideslip angle error, altitude error, and lateral error, respectively. The augmented disturbance input vector is defined as $\boldsymbol{w}_a = [\boldsymbol{r}^T \ \boldsymbol{w}^T]^T$, where the reference vector is $\boldsymbol{r} = [\beta_r \ \ \dot{h}_r \ \ d_{\text{latr}}]^T$ with β_r, h_r, and d_{latr} being the reference signals of the sideslip angle, altitude, and lateral position, respectively. The controlled output is $\boldsymbol{z} \in \boldsymbol{R}^q$, where $\boldsymbol{C}_1 \in \boldsymbol{R}^{q\times(n+p+2)}$ and $\boldsymbol{D}_1 \in \boldsymbol{R}^{q\times m}$ are constant weighting matrices, which can be adjusted to achieve satisfactory response under constraints on the deflection and the rate of deflection of the control surfaces as stated in Sec. II.B. The augmented system matrices are given as follows:

$$\boldsymbol{A}_a(\Theta) = \sum_{i=0}^{l}\boldsymbol{A}_{\text{ai}}\theta_i, \qquad \boldsymbol{B}_a(\Theta) = \sum_{i=0}^{l}\boldsymbol{B}_{\text{ai}}\theta_i, \qquad \boldsymbol{G}(\Theta) = \sum_{i=0}^{l}\boldsymbol{G}_i\theta_i \tag{24}$$

$$\boldsymbol{A}_{\text{ai}} = \left[\begin{array}{ccccc|c} 0 & 0 & 0 & 0 & 0 & -\boldsymbol{S}_1\boldsymbol{C}_{\text{pi}} \\ 0 & -\mu & 0 & 0 & 0 & -\mu\boldsymbol{S}_2\boldsymbol{C}_{\text{pi}} \\ 0 & 0 & 0 & 0 & 0 & -\boldsymbol{S}_3\boldsymbol{C}_{\text{pi}} \\ 0 & 1 & 0 & 0 & 0 & 0 \\ 0 & 0 & 0 & 1 & 0 & 0 \\ \hline 0 & 0 & 0 & 0 & 0 & \boldsymbol{A}_{\text{pi}} \end{array}\right]$$

$$\boldsymbol{B}_{\text{ai}} = \left[\begin{array}{c} 0 \\ 0 \\ 0 \\ 0 \\ 0 \\ \hline \boldsymbol{B}_{\text{pi}} \end{array}\right], \qquad \boldsymbol{G}_i = \left[\begin{array}{ccc|c} 1 & 0 & 0 & 0 \\ 0 & \mu & 0 & 0 \\ 0 & 0 & 1 & 0 \\ 0 & 0 & 0 & 0 \\ 0 & 0 & 0 & 0 \\ \hline 0 & 0 & 0 & \boldsymbol{G}_{\text{pi}} \end{array}\right] \tag{25}$$

with $\boldsymbol{S}_1 = [1 \ 0 \ 0]$, $\boldsymbol{S}_2 = [0 \ 1 \ 0]$, and $\boldsymbol{S}_3 = [0 \ 0 \ 1]$.

Obviously, if a controller can stabilize the augmented system (23), it can also stabilize the system (17) and guarantee the tracking errors to be zero.

Figure 4 gives block diagram of aircraft automatic landing control system where the tracking signals are the sideslip angle β, aircraft altitude h, and lateral error d_{lat}.

IV. Reliable Automatic Landing Control

The automatic landing control studied in this paper is based on differential global positioning system/inertial navigation system radio altimeter navigation. The state variables in Eq. (17) can all be obtained either by direct or indirect measurement. Hence we assume state-feedback in this study. Consider the following state-feedback controller for the augmented system (23):

$$\boldsymbol{u} = \boldsymbol{K}\boldsymbol{x}_a \tag{26}$$

The closed-loop system is

$$\boldsymbol{\Pi}: \begin{cases} \dot{\boldsymbol{x}}_a = [\boldsymbol{A}_a(\Theta) + \boldsymbol{B}_a(\Theta)\boldsymbol{K}]\boldsymbol{x}_a + \boldsymbol{G}(\Theta)\boldsymbol{w}_a \\ \boldsymbol{z} = (\boldsymbol{C}_1 + \boldsymbol{D}_1\boldsymbol{K})\boldsymbol{x}_a \end{cases} \tag{27}$$

where $\Theta \in \boldsymbol{\Theta}$ satisfies Eq. (18), and $\boldsymbol{A}_a(\Theta)$, $\boldsymbol{B}_a(\Theta)$, and $\boldsymbol{G}(\Theta)$ are as in Eq. (24).

The reliable robust automatic landing problem is to find a state-feedback controller (26) such that the following applies:

1) During normal operation where $\theta_0 = 1$ and $\theta_i = 0$ $(i = 1, 2, \ldots, l)$ for $\Theta \in \boldsymbol{\Theta}$, the closed-loop system $\boldsymbol{\Pi}$ is stable, and

$$\left\|\boldsymbol{\Pi}_{\text{zw}_a0}(s)\right\|_2 < \nu_0 \tag{28}$$

where $\nu_0 > 0$ and

$$\boldsymbol{\Pi}_{\text{zw}_a0}(s) := (\boldsymbol{C}_1 + \boldsymbol{D}_1\boldsymbol{K})[s\boldsymbol{I} - \boldsymbol{A}_{a0} - \boldsymbol{B}_{a0}\boldsymbol{K}]^{-1}\boldsymbol{G}_0 \tag{29}$$

2) For the ith ($i=1,\ldots,l$) vertex stuck fault where $\theta_i=1$ and $\theta_j=0$ ($j\neq i$), the closed-loop system $\mathbf{\Pi}$ is stable, and

$$\left\|\mathbf{\Pi}_{\mathrm{zw}_a i}(s)\right\|_2 < \nu_i \tag{30}$$

where $\nu_i \geq \nu_0 > 0$ and

$$\mathbf{\Pi}_{\mathrm{zw}_a i}(s) := (\boldsymbol{C}_1+\boldsymbol{D}_1\boldsymbol{K})[s\boldsymbol{I}-\boldsymbol{A}_{\mathrm{ai}}-\boldsymbol{B}_{\mathrm{ai}}\boldsymbol{K}]^{-1}\boldsymbol{G}_i \tag{31}$$

3) For any intermediate stuck fault, the closed-loop system $\mathbf{\Pi}$ is stable, and

$$\left\|\mathbf{\Pi}_{\mathrm{zw}_a}(s)\right\|_2 < \sqrt{\sum_{i=0}^{l}\theta_i\nu_i^2} < \max_{1\leq i\leq l}\nu_i \tag{32}$$

where, for $\Theta\in\mathbf{\Theta}$,

$$\mathbf{\Pi}_{\mathrm{zw}_a}(s) := (\boldsymbol{C}_1+\boldsymbol{D}_1\boldsymbol{K})[s\boldsymbol{I}-\boldsymbol{A}_a(\Theta)-\boldsymbol{B}_a(\Theta)\boldsymbol{K}]^{-1}\boldsymbol{G}(\Theta) \tag{33}$$

Note that $\nu_0 \leq \min_{1\leq i\leq l}\nu_i$. Hence the system is at its best when there is no fault and deteriorates when faults occur.

In the following, a sufficient condition for the solvability of the reliable robust autolanding control problem is given by Lemma 4.1.

Lemma 4.1 (Ref. 17): Consider the augmented system (23) with Eqs. (24) and (25), and let ν be a positive constant. Suppose that there exist symmetric matrices $\boldsymbol{Y}>0$ and $\boldsymbol{Q}>0$, and a matrix $\boldsymbol{Z}\in\boldsymbol{R}^{m\times(n+p+2)}$ such that the following LMIs hold for all $i=0,1,\ldots,l$:

$$\begin{bmatrix}\boldsymbol{A}_{\mathrm{ai}}\boldsymbol{Y}+\boldsymbol{Y}\boldsymbol{A}_{\mathrm{ai}}^T+\boldsymbol{B}_{\mathrm{ai}}\boldsymbol{Z}+\boldsymbol{Z}^T\boldsymbol{B}_{\mathrm{ai}}^T & \boldsymbol{Y}\boldsymbol{C}_1^T+\boldsymbol{Z}^T\boldsymbol{D}_1^T\\ \boldsymbol{C}_1\boldsymbol{Y}+\boldsymbol{D}_1\boldsymbol{Z} & -\boldsymbol{I}\end{bmatrix}<0 \tag{34}$$

$$\begin{bmatrix}\boldsymbol{Y} & \boldsymbol{G}_i\\ \boldsymbol{G}_i^T & \boldsymbol{Q}\end{bmatrix}>0 \tag{35}$$

$$\mathrm{trace}(\boldsymbol{Q})<\nu^2 \tag{36}$$

Then the state-feedback controller $\boldsymbol{u}=\boldsymbol{K}\boldsymbol{x}_a$ with $\boldsymbol{K}=\boldsymbol{Z}\boldsymbol{Y}^{-1}$ stabilizes the augmented system (23) and achieves that $\|\mathbf{\Pi}_{\mathrm{zw}_a}(s)\|_2<\nu$.

Remark 4.1: The sufficient conditions (34–36) given in Lemma 4.1 are very conservative as only a single common Lyapunov matrix $\boldsymbol{Y}$ is used for both the normal ($i=0$) and fault ($i=1,2,\ldots,l$) systems. By Lemma 4.1, it is also difficult to distinguish performance of the normal system and faulty systems. Accordingly, it is difficult to optimize the performance of the normal system under the constraints of upper bounds of faulty system performance.

To reduce the conservativeness in controller design, the following affine parameter-dependent Lyapunov functions are adopted:

$$\mathcal{V}_2(\boldsymbol{x},\Theta)=\boldsymbol{x}^T\boldsymbol{X}(\Theta)\boldsymbol{x},\qquad \Theta\in\mathbf{\Theta} \tag{37}$$

where $\boldsymbol{X}(\Theta)$ is an affine function of $\Theta\in\mathbf{\Theta}$, that is,

$$\boldsymbol{X}(\Theta)=\sum_{i=0}^{l}\boldsymbol{X}_i\theta_i \tag{38}$$

with $\boldsymbol{X}_i>0$ for $i=0,1,\ldots,l$.

Remark 4.2: Note that when $\boldsymbol{X}_0=\boldsymbol{X}_1=\cdots=\boldsymbol{X}_l=\boldsymbol{X}$, we have that $\boldsymbol{X}(\Theta)=\boldsymbol{X}$ and $\mathcal{V}_2(\boldsymbol{x},\Theta)=\boldsymbol{x}^T\boldsymbol{X}\boldsymbol{x}$, which is simply the quadratic stability result.[18] Therefore solutions based on affine parameter-dependent Lyapunov functions are at most as conservative as those based on single Lyapunov functions (i.e., Lemma 4.1).

Before presenting the main results, an important lemma is given in the following. Let

$$\boldsymbol{A}(\Theta)=\boldsymbol{A}_a(\Theta)+\boldsymbol{B}_a(\Theta)\boldsymbol{K},\qquad \boldsymbol{C}=\boldsymbol{C}_1+\boldsymbol{D}_1\boldsymbol{K} \tag{39}$$

Then the closed-loop system (27) can be rewritten as follows:

$$\mathbf{\Pi}:\begin{cases}\dot{\boldsymbol{x}}_a=\boldsymbol{A}(\Theta)\boldsymbol{x}_a+\boldsymbol{G}(\Theta)\boldsymbol{w}_a\\ \boldsymbol{z}=\boldsymbol{C}\boldsymbol{x}_a\end{cases} \tag{40}$$

Lemma 4.2 (Ref. 19): For a given positive constant ν, the system $\mathbf{\Pi}$ as in Eq. (40) is stable and $\|\mathbf{\Pi}_{\mathrm{zw}_a}(s)\|_2<\nu$ if there exist symmetric positive-definite matrices $\boldsymbol{X}(\Theta)$ as in Eq. (38) and $\boldsymbol{Q}(\Theta)$, and a matrix $\boldsymbol{V}$ such that

$$\begin{bmatrix}-(\boldsymbol{V}+\boldsymbol{V}^T) & \boldsymbol{V}^T\boldsymbol{A}^T(\Theta)+\boldsymbol{X}(\Theta) & \boldsymbol{V}^T\boldsymbol{C}^T & \boldsymbol{V}^T\\ \boldsymbol{A}(\Theta)\boldsymbol{V}+\boldsymbol{X}(\Theta) & -\boldsymbol{X}(\Theta) & 0 & 0\\ \boldsymbol{C}\boldsymbol{V} & 0 & -\boldsymbol{I} & 0\\ \boldsymbol{V} & 0 & 0 & -\boldsymbol{X}(\Theta)\end{bmatrix}<0 \tag{41}$$

$$\begin{bmatrix}\boldsymbol{X}(\Theta) & \boldsymbol{G}(\Theta)\\ \boldsymbol{G}^T(\Theta) & \boldsymbol{Q}(\Theta)\end{bmatrix}>0,\qquad \mathrm{trace}[\boldsymbol{Q}(\Theta)]<\nu^2 \tag{42}$$

where

$$\boldsymbol{Q}(\Theta)=\sum_{i=0}^{l}\boldsymbol{Q}_i\theta_i \tag{43}$$

Remark 4.3: Lemma 4.2 gives sufficient conditions for the affine quadratic H_2 performance test. Moreover, the conditions given in Eqs. (41) and (42) are linear matrix inequalities that can be easily solved by using existing LMI Tool Box.[20]

According to Lemma 4.2, a design method of reliable H_2 autolanding controller is presented in the following theorem.

Theorem 4.1: Consider the augmented system (23) with Eqs. (24) and (25), and let ν_i ($i=0,1,\ldots,l$) be positive constants with $\nu_0<\min_{1\leq i\leq l}\nu_i$. Suppose that there exist symmetric positive-definite matrices $\boldsymbol{X}_i$ as in Eq. (38) and $\boldsymbol{Q}_i$ as in Eq. (43), and matrices $\boldsymbol{W}$ and $\boldsymbol{V}$ such that the following LMIs hold for all $i=0,1,\ldots,l$:

$$\begin{bmatrix}-(\boldsymbol{V}+\boldsymbol{V}^T) & \boldsymbol{V}^T\boldsymbol{A}_{\mathrm{ai}}^T+\boldsymbol{W}^T\boldsymbol{B}_{\mathrm{ai}}^T+\boldsymbol{X}_i & \boldsymbol{V}^T\boldsymbol{C}_1^T+\boldsymbol{W}^T\boldsymbol{D}_1^T & \boldsymbol{V}^T\\ \boldsymbol{A}_{\mathrm{ai}}\boldsymbol{V}+\boldsymbol{B}_{\mathrm{ai}}\boldsymbol{W}+\boldsymbol{X}_i & -\boldsymbol{X}_i & 0 & 0\\ \boldsymbol{C}_1\boldsymbol{V}+\boldsymbol{D}_1\boldsymbol{W} & 0 & -\boldsymbol{I} & 0\\ \boldsymbol{V} & 0 & 0 & -\boldsymbol{X}_i\end{bmatrix}<0 \tag{44}$$

$$\begin{bmatrix}\boldsymbol{X}_i & \boldsymbol{G}_i\\ \boldsymbol{G}_i^T & \boldsymbol{Q}_i\end{bmatrix}>0 \tag{45}$$

$$\mathrm{trace}(\boldsymbol{Q}_i)<\nu_i^2 \tag{46}$$

Then the state-feedback controller $\boldsymbol{u}=\boldsymbol{K}\boldsymbol{x}_a$ with $\boldsymbol{K}=\boldsymbol{W}\boldsymbol{V}^{-1}$ stabilizes the augmented system (23) and achieves that $\|\mathbf{\Pi}_{\mathrm{zw}_a 0}(s)\|_2<\nu_0$, $\|\mathbf{\Pi}_{\mathrm{zw}_a i}(s)\|_2<\nu_i$ ($i=1,2,\ldots,l$) and

$$\|\mathbf{\Pi}_{\mathrm{zw}_a}(s)\|_2 < \sqrt{\sum_{i=0}^{l}\theta_i\nu_i^2} < \max_{1\leq i\leq l}\nu_i$$

Proof: By substituting Eqs. (24) and (39) into Eq. (41) in Lemma 4.2 and letting $\boldsymbol{W} = \boldsymbol{KV}$, Theorem 4.1 is obvious. □

The reliable autolanding control problem under consideration can be restated as follows: For given H_2 upper bounds ν_i $(i = 1, 2, \ldots, l)$ of the closed-loop system in the fault cases, minimize ν_0 subject to LMIs (44–46), where ν_0 is the H_2 upper bound of the closed-loop system under the normal operation.

After choosing

$$\boldsymbol{C}_1 = \begin{bmatrix} \boldsymbol{C}_{11} & 0_{5\times 10} \\ 0_{5\times 5} & 0_{5\times 10} \end{bmatrix}, \qquad \boldsymbol{D}_1 = \begin{bmatrix} 0_{5\times 5} \\ \boldsymbol{I}_{5\times 5} \end{bmatrix}$$

$$\boldsymbol{C}_{11} = \text{diag}\,\{0.5, 2, 0.5, 2, 4\} \tag{47}$$

we obtain a reliable state-feedback control law

$$\boldsymbol{u} = \boldsymbol{K}_{\text{reliable}} \left[\int_0^t e_\beta \,\mathrm{d}t \quad \dot{e}_h \quad \int_0^t e_{\text{lat}} \,\mathrm{d}t \quad e_h \quad \int_0^t e_h \,\mathrm{d}t \quad u \quad w \quad q \quad \theta \quad v \quad p \quad r \quad \phi \quad \psi \quad P_E \right]^T \tag{48}$$

with

$$\boldsymbol{K}_{\text{reliable}} = \begin{bmatrix} 0.0597 & -0.3890 & 0.1935 & -5.6802 & -2.1977 & 1.8455 & -4.2890 & 90.2642 \\ -0.0550 & -0.3899 & -0.1938 & -5.6957 & -2.2066 & 1.8488 & -4.2934 & 89.9973 \\ 0.1083 & 0.1595 & 0.3441 & 2.9444 & 1.3306 & -0.7056 & 1.8534 & -20.0232 \\ -0.1100 & 0.1570 & -0.3431 & 2.8804 & 1.3038 & -0.6896 & 1.8212 & -20.1163 \\ 0.4516 & 0.0041 & -0.2241 & 0.0821 & 0.0289 & -0.0203 & 0.0516 & 0.1955 \end{bmatrix}$$

$$\begin{bmatrix} 579.4353 & -1.6313 & -6.3845 & -22.2724 & 9.2600 & -172.6681 & -0.8932 \\ 580.3961 & 1.6402 & 6.5196 & 21.6981 & -9.1906 & 173.3939 & 0.8957 \\ -239.1949 & -3.0131 & -16.7692 & -58.6250 & 16.6784 & -333.5391 & -1.6462 \\ -234.3086 & 2.9964 & 16.6398 & 59.0335 & -16.6528 & 332.6065 & 1.6417 \\ -6.6247 & 2.0218 & 7.9260 & 114.6763 & -18.6681 & 281.1183 & 1.2371 \end{bmatrix}$$

For the purpose of comparison, a standard H_2 autolanding controller $\boldsymbol{K}_{\text{standard}}$ without considering the fault cases and a reliable autolanding controller $\boldsymbol{K}_{\text{common}}$ by using Lemma 4.1 are also obtained.

$$\boldsymbol{K}_{\text{standard}} = \begin{bmatrix} -0.0465 & -0.2877 & 0.2520 & -5.9579 & -2.5461 & 1.5562 & -4.2387 & 75.4827 \\ 0.0513 & -0.2875 & -0.2514 & -5.9543 & -2.5454 & 1.5545 & -4.2352 & 75.4495 \\ 0.1741 & 0.1210 & 0.2302 & 2.3503 & 1.2401 & -0.4557 & 1.4521 & -13.9940 \\ -0.1748 & 0.1189 & -0.2305 & 2.3069 & 1.2193 & -0.4469 & 1.4241 & -13.7074 \\ 0.4320 & 0.0023 & -0.1270 & 0.0473 & 0.0217 & -0.0106 & 0.0318 & -0.3204 \end{bmatrix}$$

$$\begin{bmatrix} 524.0596 & -1.6212 & -4.4961 & -35.6136 & 11.9592 & -169.1134 & -1.0136 \\ 523.5393 & 1.6266 & 4.5860 & 34.9272 & -11.8641 & 168.9363 & 1.0119 \\ -162.0880 & -1.3642 & -4.1324 & -24.0390 & 9.7381 & -139.0599 & -0.8747 \\ -158.9562 & 1.3616 & 4.1050 & 24.2480 & -9.7745 & 139.2139 & 0.8758 \\ -3.6884 & 1.0379 & 2.3106 & 32.5279 & -8.1100 & 113.0472 & 0.6030 \end{bmatrix}$$

$$\boldsymbol{K}_{\text{common}} = 10^3 * \begin{bmatrix} 0.0001 & -0.0004 & 0.0003 & -0.0079 & -0.0029 & 0.0026 & -0.0059 \\ -0.0001 & -0.0004 & -0.0003 & -0.0079 & -0.0029 & 0.0027 & -0.0059 \\ 0.0000 & 0.0001 & 0.0012 & 0.0019 & 0.0007 & -0.0005 & 0.0014 \\ -0.0000 & 0.0001 & -0.0012 & 0.0017 & 0.0007 & -0.0005 & 0.0013 \\ 0.0006 & 0.0000 & -0.0010 & 0.0001 & 0.0000 & -0.0000 & 0.0000 \end{bmatrix}$$

$$\begin{bmatrix} 0.1418 & 0.8251 & -0.0034 & -0.0126 & -0.0461 & 0.0195 & -0.3587 & -0.0017 \\ 0.1421 & 0.8286 & 0.0035 & 0.0130 & 0.0471 & -0.0197 & 0.3633 & 0.0017 \\ -0.0272 & -0.1810 & -0.0117 & -0.0555 & -0.2333 & 0.0729 & -1.3046 & -0.0061 \\ -0.0256 & -0.1695 & 0.0118 & 0.0555 & 0.2336 & -0.0730 & 1.3067 & 0.0061 \\ -0.0001 & -0.0054 & 0.0099 & 0.0385 & 0.3471 & -0.0765 & 1.2173 & 0.0054 \end{bmatrix}$$

The H_2 performance indices achieved by the reliable controllers $\boldsymbol{K}_{\text{reliable}}$ and $\boldsymbol{K}_{\text{common}}$ and the standard controller $\boldsymbol{K}_{\text{standard}}$ are listed in Table 1. The designed H_2 performance indices are also listed in Table 1 for comparison. Note that the larger the gap between the designed and achieved performance indices, the more conservative the design. From Table 1, it can be observed that the quadratic-stability-based reliable controller design approach by Lemma 4.1 is quite conservative. Compared to the standard controller $\boldsymbol{K}_{\text{standard}}$, which is optimal for the normal case, the reliable controller $\boldsymbol{K}_{\text{reliable}}$ obtained by Theorem 4.1 dramatically improves the system performance in the case of the actuator stuck faults by sacrificing the normal system performance slightly from 10.8 to 11.3 (4.6%).

V. Nonlinear Simulation

The reliable controller $\boldsymbol{K}_{\text{reliable}}$ is tested on the six-degree-of-freedom nonlinear aircraft model with original wind-tunnel test

Table 1 H_2 performance indices of the reliable and standard controllers

		K_{reliable} (Theorem 4.1)		K_{standard}		K_{common} (Lemma 4.1)	
Case	H_2	Designed	Achieved	Designed	Achieved	Designed	Achieved
Normal	ν_0	12.0	11.3	10.8	10.8	16.1	11.9
δ_{al}							
Stuck at 20 deg	ν_1	<12.9	12.0	——	Unstable	16.1	12.5
Stuck at −20 deg	ν_2	<12.9	11.7	——	11.0	16.1	12.1
δ_{ar}							
Stuck at 20 deg	ν_3	<12.9	12.0	——	Unstable	16.1	12.5
Stuck at −20 deg	ν_4	<12.9	11.9	——	Unstable	16.1	12.4
δ_{hl}							
Stuck at 0 deg	ν_5	<12.9	12.4	——	14.9	16.1	12.9
δ_{hr}							
Stuck at 0 deg	ν_6	<12.9	12.4	——	14.8	16.1	12.9

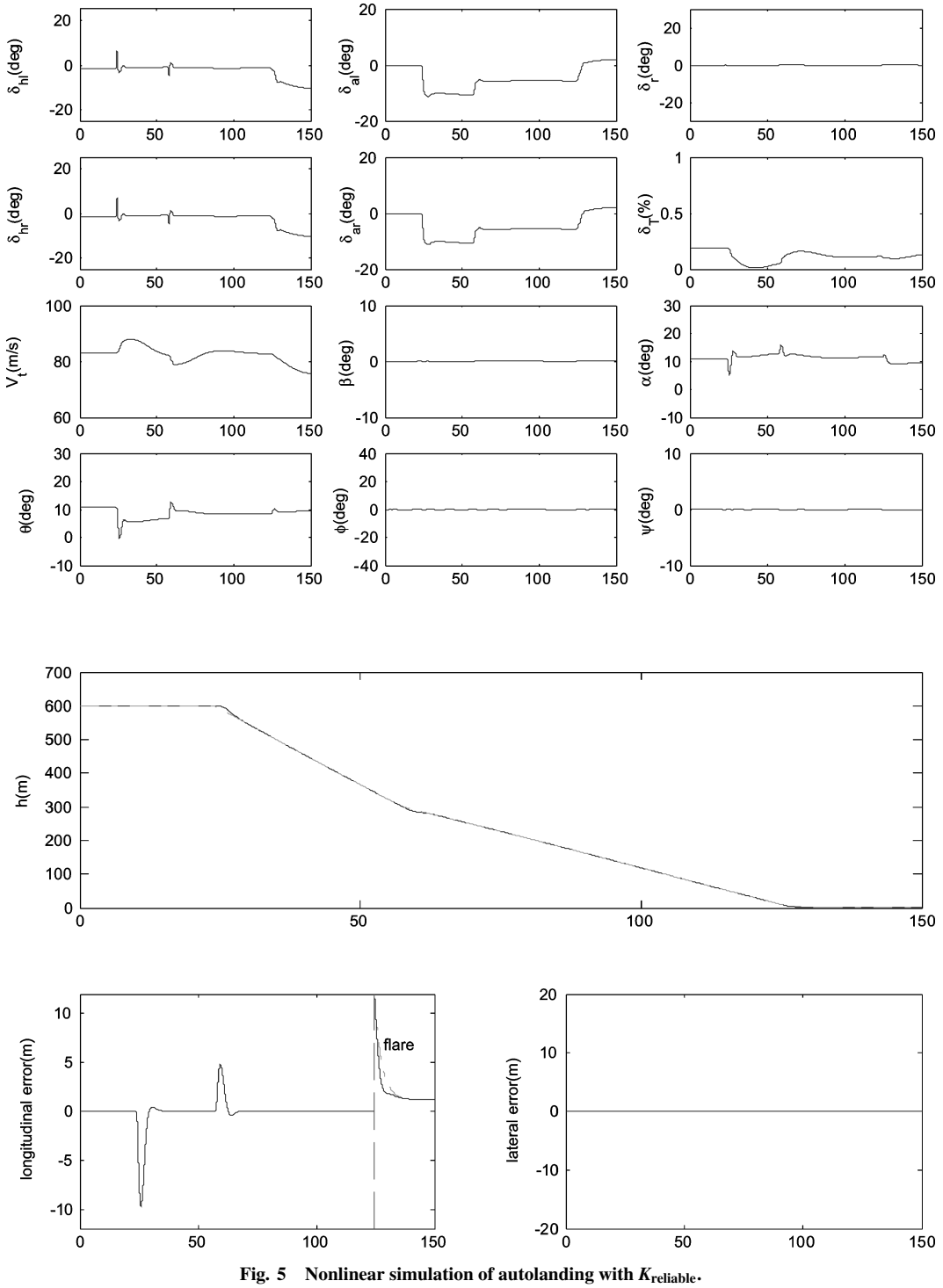

Fig. 5 Nonlinear simulation of autolanding with K_{reliable}.

data and computational-fluid-dynamics data (see Sec. II.A for details). Landing-gear effects and ground effects are included in the nonlinear aircraft model. Aircraft airspeed is controlled by adjusting throttle δ_T according to the following throttle control law:

$$\delta_T = 0.0017 \int_0^t (V_{\text{tr}} - V_t)\,\mathrm{d}t - 0.0157u - 0.0036w \qquad (49)$$

where V_{tr} is the reference signal of the airspeed V_t.

Assume the runway lies in the northward direction. Simulations of the autolanding process are done in the following sequence: First, the aircraft keeps a northward wing-level flight at the height of 600 m. After 2-km northward flight, the glide-slope mode is engaged to track the glide path with flight-path angle $\Gamma = -6$ deg until the flight height reaches 300 m. Then the glide slope of $\Gamma = -3$ deg is tracked. Once the flight height reaches 12 m, the glide-slope mode is disengaged, and the flare mode is engaged until the aircraft touches down. The airspeed hold mode controlled by the engine throttle is engaged during the whole autolanding process. During wing-level flight and glide-slope segment, the airspeed is maintained at 82.88 m/s. During the flare segment, the airspeed reduces to 76.19 m/s, and the sink rate at touchdown is 0.4 m/s.

SIMULINK in MATLAB® 6.1 is used to simulate the whole autolanding process controlled by the reliable controller $\boldsymbol{K}_{\text{reliable}}$. In addition to considering the wind disturbances described in Sec. II.D,

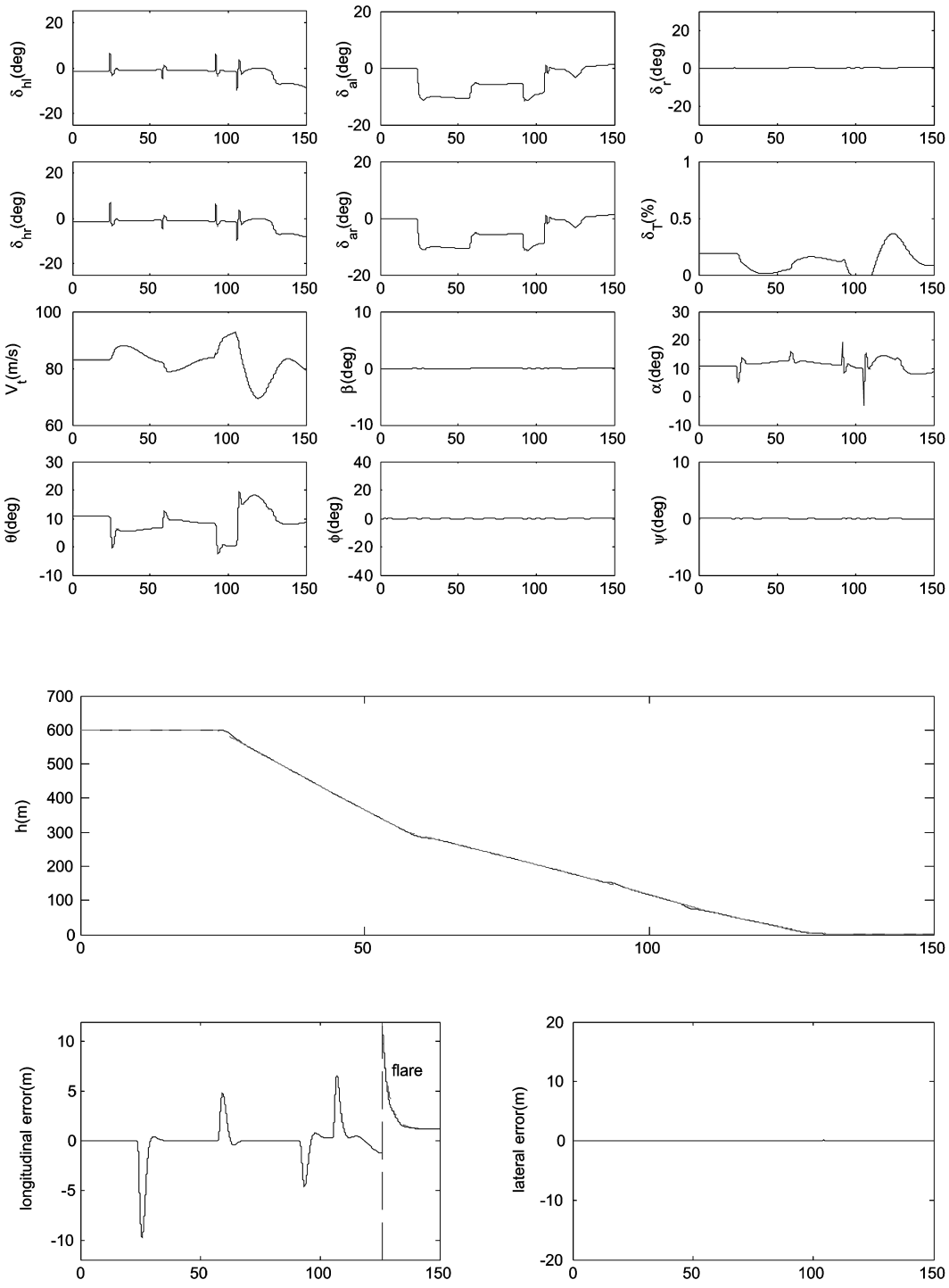

Fig. 6 Nonlinear simulation of autolanding with the vertical wind shear as in Fig. 3.

stuck faults among the left and right ailerons and horizontal stabilators are also included in the simulation.

Figure 5 gives the responses of the control ($\delta_{\rm hl}$, $\delta_{\rm hr}$, $\delta_{\rm al}$, $\delta_{\rm al}$, δ_r, and δ_T), velocity V_t, angle of sideslip β, angle of attack α, attitude (θ, ϕ and ψ), and altitude h as well as longitudinal error ($d_{\rm lon} = h_r - h$), and lateral error $d_{\rm lat}$ signals of the aircraft under the normal operation without wind disturbance. The simulation results show that the designed reliable autolanding controller $\boldsymbol{K}_{\rm reliable}$ achieves zero steady-state tracking error and good tracking response with the longitudinal error

$$d_{\rm lon} \le \begin{cases} 0.5\,{\rm m}, & h < 150\,{\rm m} \\ 5\,{\rm m}, & 150\,{\rm m} < h < 500\,{\rm m} \\ 10\,{\rm m}, & h > 500\,{\rm m} \end{cases} \tag{50}$$

and the lateral error $d_{\rm lat} \le 0.1$ m in the normal case without wind disturbance (see plots of longitudinal error and lateral error in Fig. 5 for details). In the plot of longitudinal error, instead of the longitudinal error, the actual flare exponential curve (solid line) is given for the flare phase, which is separated by a vertical dash line. The dash–dot lines in the plots of h and longitudinal error represent the altitude and flare command profile, respectively. The preceding statements are applicable to all of Figs. 5–11.

As is well known, low-altitude wind shear has been recognized as a serious threat to the safety of aircraft in landing. Figure 6 shows the simulation results under wind shear as shown in Fig. 3. Here the wind is suddenly increased to -40 ft/s (-12.2 m/s, vertically upward) from 0 ft/s at altitude 510 ft (155.4 m) when $t = 92$ s and changes abruptly to 35 ft/s (10.7 m/s, vertically downward) at altitude 300 ft

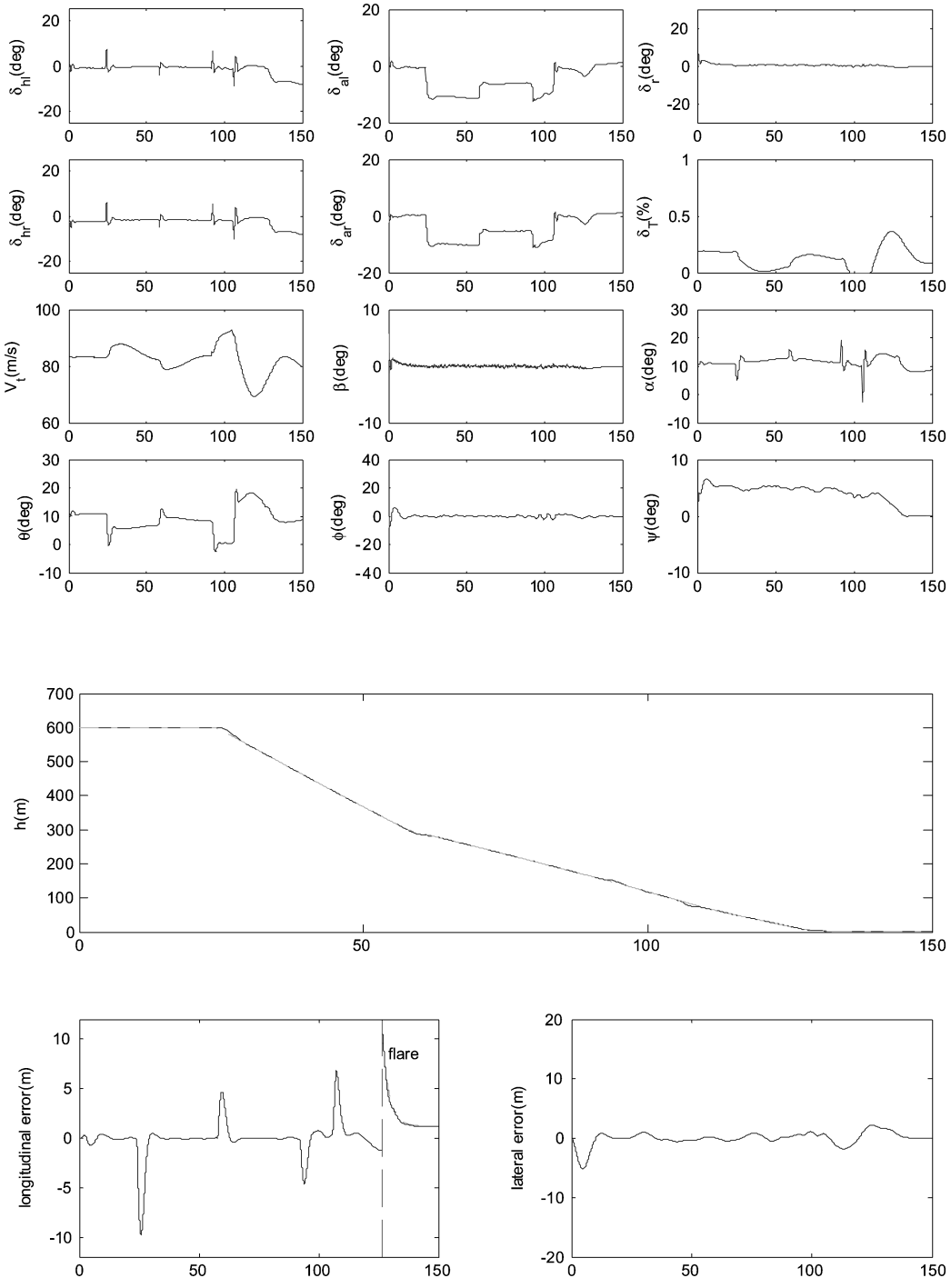

Fig. 7 Nonlinear simulation of autolanding with the vertical wind shear as in Fig. 3 and the lateral turbulence as in Fig. 2.

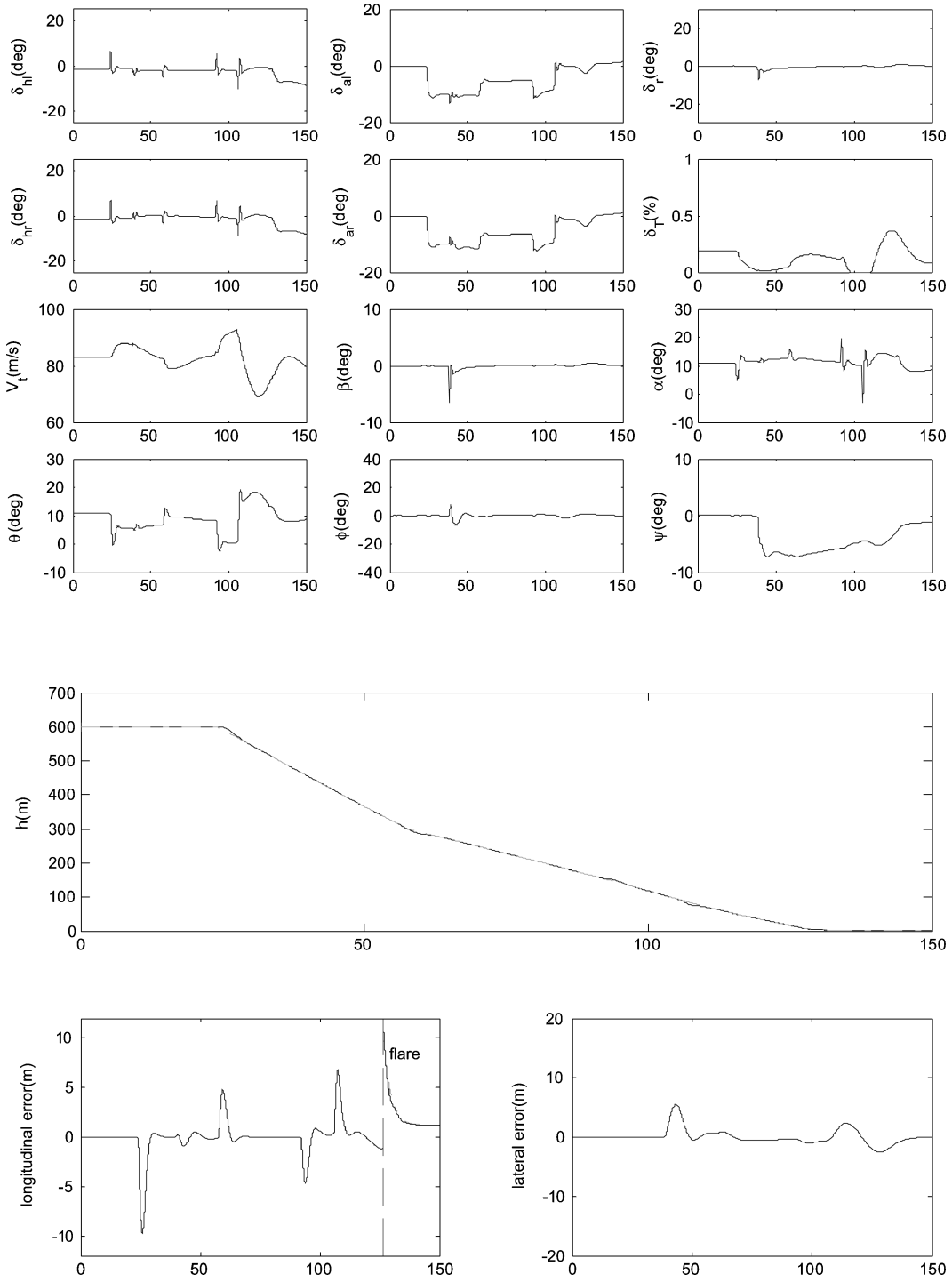

Fig. 8 Nonlinear simulation of autolanding with the vertical wind shear as in Fig. 3 and the lateral deterministic wind as in Fig. 1.

(91.4 m) when $t = 105$ s. For the severe wind-shear simulation, the strong sudden wind of -40 ft/s (-12.2 m/s) causes the angle of attack α to increase suddenly by about 8 deg. This strong wind persists until about $t = 105$ s at an altitude 300 ft (91.4 m), when it suddenly changes direction to 35 ft/s (10.7 m/s). It can be seen that the controller performs very well in handling the wind shear, and the longitudinal error between the desired path and the actual path is kept within 10 m and the lateral error is kept within 0.1 m. Figure 7 gives the simulation results under the vertical wind shear of Fig. 3 and the lateral turbulence of Fig. 2. Figure 8 gives the autolanding simulation results under the vertical wind shear of Fig. 3 and the lateral deterministic wind of Fig. 1. It is observed that lateral wind causes a nonzero aircraft heading angle ψ. To track the glide path, there must be a tradeoff between heading angle and angle of sideslip β in the case of lateral wind. In other words, if the angle of sideslip is forced to be zero, the heading angle can be eliminated only if the lateral wind disappears. The simulation results show that the aircraft is stabilized and manipulated well under strong vertical and lateral winds. The longitudinal error is kept within 10 m, and the lateral error is kept within 5 m. Hence, the reliable autolanding controller $\boldsymbol{K}_{\text{reliable}}$ is quite robust for wind disturbances.

In the process of autolanding, reliability against faults is another important requirement. Figure 9 gives the simulation results of the autolanding aircraft when its right horizontal stabilator is suddenly

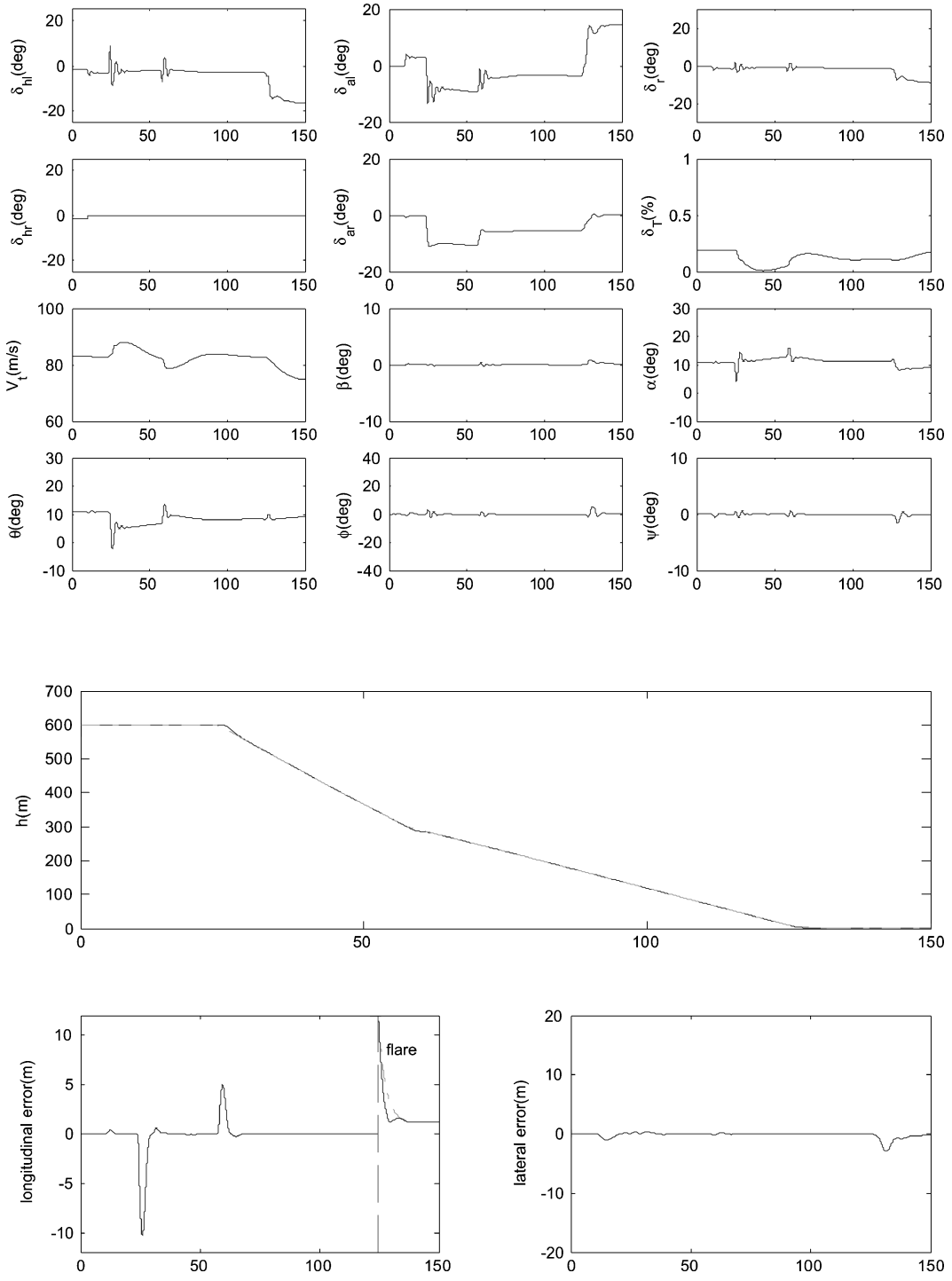

Fig. 9 Nonlinear simulation with the δ_{hr} stuck at 0 deg.

stuck at 0 deg at $t = 10$ s onward. It can be seen that the controller performs well in handling the horizontal stabilator stuck fault with the longitudinal error satisfying Eq. (50) and the lateral error kept within 2.5 m. Figure 10 displays the simulation results with the left aileron of the aircraft stuck at -20 deg at $t = 10$ s and with the lateral turbulence of Fig. 2 acting on the aircraft. In addition, the simulation results with the right aileron stuck at 20 deg at $t = 10$ s and the lateral deterministic wind of Fig. 1 acting on the aircraft are given in Fig. 11. It can be seen from Figs. 10 and 11 that the longitudinal error also satisfies Eq. (50) and the lateral error is kept within 10 m. As there are many combination cases of wind disturbances and actuator stuck faults, here they will not be listed one by one although they have all been tested.

Simulations of measurement noises/inaccuracies in the state variables u, v, w, p, q, r, θ, ϕ, ψ, and P_E have also been done. Simulation results show that the reliable autolanding controller $\boldsymbol{K}_{\mathrm{reliable}}$ performs well under measurement noises/inaccuracies. In fact, the effect of measurement noises/inaccuracies in u, v, and w is similar to that of wind. The plots are not given here. Moreover, simulation results show that the reliable landing controller $\boldsymbol{K}_{\mathrm{reliable}}$ can tolerate X_{cg} variation from $0.27\bar{c}$ to $0.39\bar{c}$, mass variation upto 40%, control time delay up to 120 ms, and speed variation from 65 to 110 m/s. (The reference center-of-gravity position is at $X_{\mathrm{rcg}} = 0.35\bar{c}$.)

In summary, all simulation results show that the fixed single reliable autolanding controller $\boldsymbol{K}_{\mathrm{reliable}}$ works well during the whole landing process, including the wing-level flight, glide-slope flights

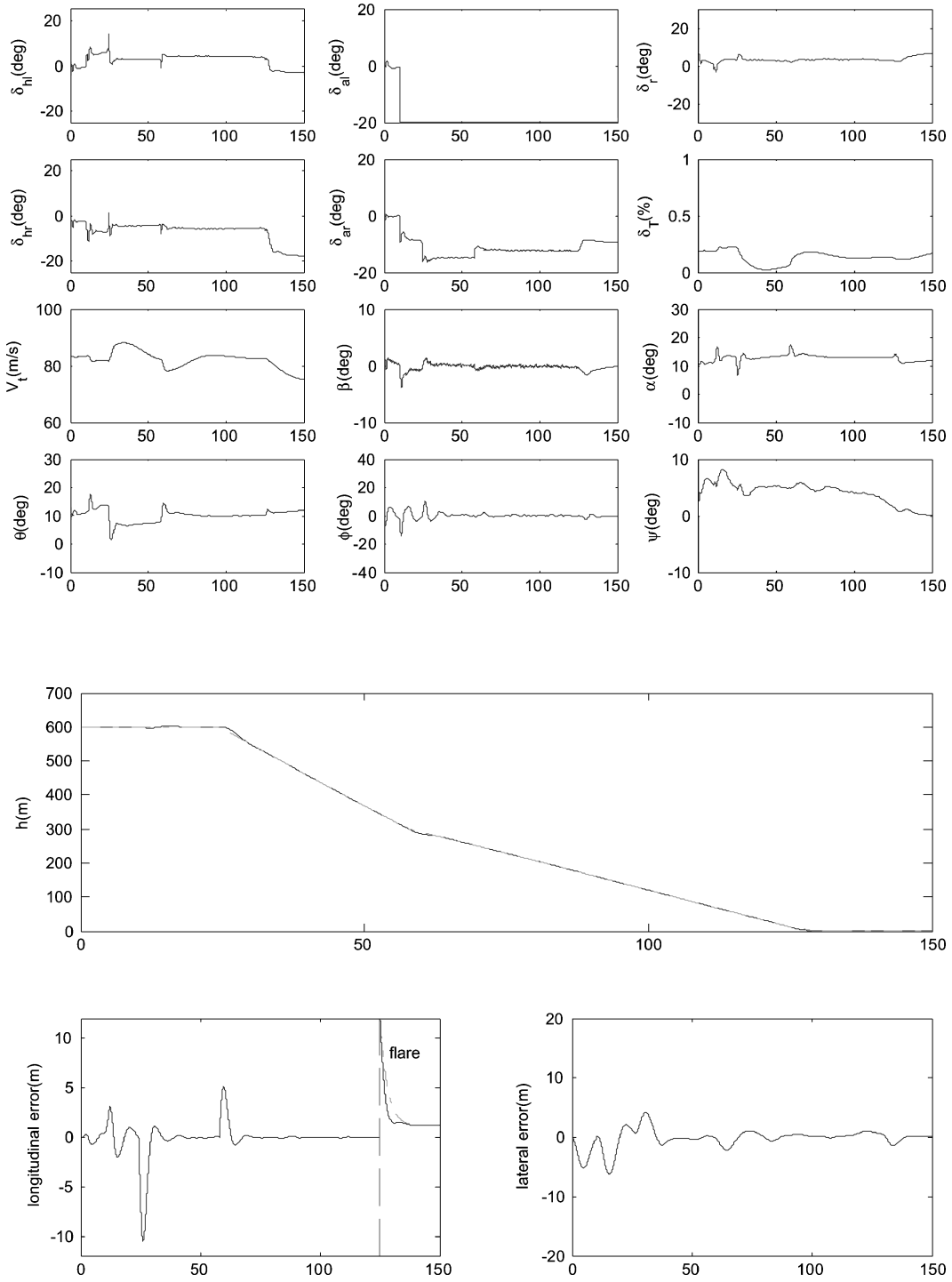

Fig. 10 Nonlinear simulation of autolanding with the δ_{al} stuck at −20 deg and the lateral turbulence as in Fig. 2.

of 6 and 3 deg, and flare. Furthermore, the reliable autolanding controller $\boldsymbol{K}_{\text{reliable}}$ performs very well not only in rejecting wind disturbances and measurement noises, but also in handling actuator stuck faults.

Unlike conventional autolanding controllers that mandate differential deflection of ailerons and synchronous deflection of horizontal stabilators, the designed reliable controller has all control surfaces (the left and right ailerons and the left and right horizontal stabilators, as well as the rudder) deflecting independently. The control principle of the reliable controller is as follows. When the left (right) aileron is stuck, the right (left) aileron deflects in the same direction to compensate partially the rolling moment caused by the left (right) stuck aileron so that the left and right horizontal stabilators and the rudder have enough control authority to balance the remaining pitching moment, rolling moment, and yawing moment caused by the stuck aileron (see Figs. 10 and 11). Similarly, when the left (right) horizontal stabilator is stuck (see Fig. 9), the right (left) horizontal stabilator deflects in the opposite direction to compensate partially the pitching moment caused by the left (right) stuck horizontal stabilator so that the left and right ailerons and the rudder have enough control authority to balance the remaining pitching moment, rolling moment, and yawing moment caused by the stuck horizontal stabilator. Hence,

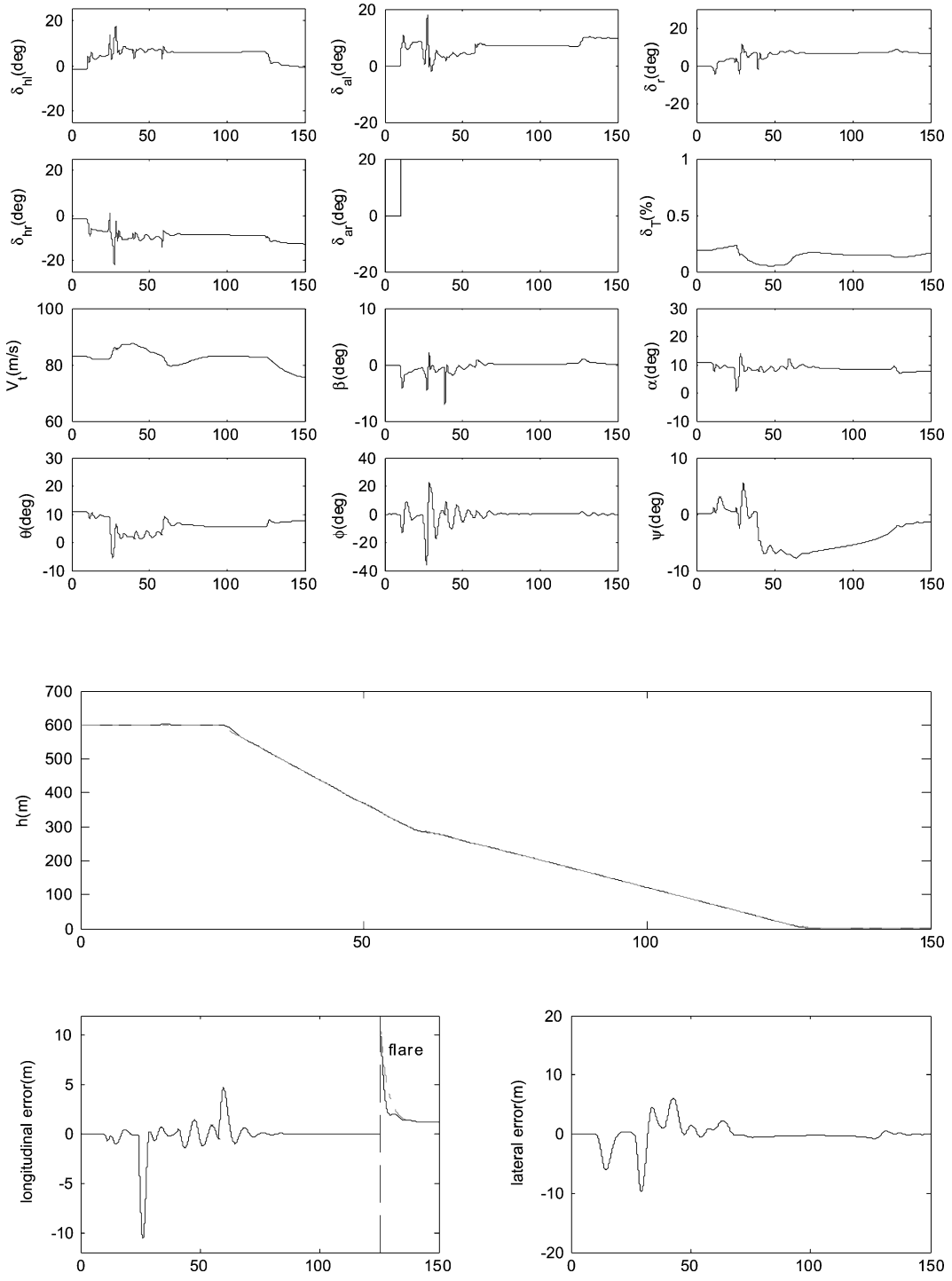

Fig. 11 Nonlinear simulation of autolanding with the δ_{ar} stuck at 20 deg and the lateral deterministic wind as in Fig. 1.

although the conventional control surface deflection can control the aircraft quite effectively in normal operation according to symmetry of the aircraft, the independent control surface deflection can provide more flexible and effective control to tolerate severe actuator stuck faults.

VI. Conclusions

This paper considers the reliable automatic landing control problem against actuator stuck faults. An H_2 reliable controller design approach has been presented to solve this problem in terms of linear matrix inequalities. To demonstrate the approach, a fixed single reliable automatic landing controller is designed for a high-fidelity fighter aircraft model by using the proposed approach. Nonlinear simulation results show that the single fixed reliable autolanding controller can effectively handle tracking accuracy and robustness against wind disturbances and reliability against actuator stuck faults during the whole landing process. Moreover, the approach proposed in this paper can readily be applied to the design of reliable controllers against control surface impairment faults.

Appendix: System Matrices

$$\boldsymbol{A}_{p0} = \begin{bmatrix} -0.0210 & 0.1302 & -15.0406 & -9.6305 & -0.0012 & 0 & 0 & 0 & 0 & 0 \\ -0.1178 & -0.6136 & 73.6660 & -1.8681 & -0.0054 & 0 & 0 & 0 & 0 & 0 \\ 0.0001 & 0 & -0.6461 & 0 & -0.0001 & 0 & -0.0029 & 0 & 0 & 0 \\ 0 & 0 & 1.0000 & 0 & 0 & 0 & 0 & 0 & 0 & 0 \\ 0 & 0 & 0 & 0 & -0.1474 & 15.9764 & -80.7097 & 9.6305 & 0 & 0 \\ 0 & 0 & 0.0003 & 0 & -0.1687 & -1.7569 & 0.8767 & 0 & 0 & 0 \\ 0 & 0 & 0.0025 & 0 & 0.0223 & -0.0482 & -0.2402 & 0 & 0 & 0 \\ 0 & 0 & 0 & 0 & 0 & 1.0000 & 0.1940 & 0 & 0 & 0 \\ 0 & 0 & 0 & 0 & 0 & 0 & 1.0186 & 0 & 0 & 0 \\ 0 & 0 & 0 & 0 & 1.0000 & 0 & 0 & -15.7825 & 82.8800 & 0 \end{bmatrix}$$

$$\boldsymbol{B}_{p0} = \begin{bmatrix} 0.0075 & 0.0075 & -0.0010 & -0.0010 & 0 \\ -0.0674 & -0.0674 & -0.0679 & -0.0680 & 0 \\ -0.0301 & -0.0301 & 0.0004 & 0.0004 & 0 \\ 0 & 0 & 0 & 0 & 0 \\ -0.0154 & 0.0154 & 0.0011 & -0.0011 & 0.0336 \\ 0.0562 & -0.0562 & 0.0844 & -0.0844 & 0.0340 \\ 0.0084 & -0.0084 & 0.0008 & -0.0008 & -0.0169 \\ 0 & 0 & 0 & 0 & 0 \\ 0 & 0 & 0 & 0 & 0 \\ 0 & 0 & 0 & 0 & 0 \end{bmatrix}, \quad \boldsymbol{G}_{p0} = \begin{bmatrix} -0.0210 & 0.1302 & -0.0012 \\ -0.1178 & -0.6136 & -0.0054 \\ 0.0001 & 0 & -0.0001 \\ 0 & 0 & 0 \\ 0 & 0 & -0.1474 \\ 0 & 0 & -0.1687 \\ 0 & 0 & 0.0223 \\ 0 & 0 & 0 \\ 0 & 0 & 0 \\ 0 & 0 & 1.0000 \end{bmatrix}$$

$$\boldsymbol{C}_{p0} = \begin{bmatrix} 0 & 0 & 0 & 0 & 0.6913 & 0 & 0 & 0 & 0 & 0 \\ 0.1904 & -0.9817 & 0 & 82.8800 & 0 & 0 & 0 & 0 & 0 & 0 \\ 0 & 0 & 0 & 0 & 0 & 0 & 0 & 0 & 0 & 1.0000 \end{bmatrix}$$

$$\boldsymbol{A}_{p1} = \begin{bmatrix} -0.0269 & 0.1010 & -10.9645 & -9.7139 & -0.0010 & 0 & 0 & 0 & 0 & 0 \\ -0.1624 & -0.5282 & 74.3778 & -1.3695 & -0.0023 & 0 & 0 & 0 & 0 & 0 \\ -0.0009 & 0.0068 & -0.6088 & 0 & -0.0001 & 0 & -0.0029 & 0 & 0 & 0 \\ 0 & 0 & 1.0000 & 0 & 0 & 0 & 0 & 0 & 0 & 0 \\ 0 & 0 & 0 & 0 & -0.1518 & 11.7055 & -81.4323 & 9.7139 & 0 & 0 \\ 0 & 0 & 0.0003 & 0 & -0.1475 & -1.7875 & 0.6768 & 0 & 0 & 0 \\ 0 & 0 & 0.0025 & 0 & 0.0246 & -0.0426 & -0.2379 & 0 & 0 & 0 \\ 0 & 0 & 0 & 0 & 0 & 1.0000 & 0.1410 & 0 & 0 & 0 \\ 0 & 0 & 0 & 0 & 0 & 0 & 1.0099 & 0 & 0 & 0 \\ 0 & 0 & 0 & 0 & 1.0000 & 0 & 0 & -11.5700 & 82.8800 & 0 \end{bmatrix}$$

$$\boldsymbol{B}_{p1} = \begin{bmatrix} 0.0135 & 0.0135 & 0 & -0.0066 & 0 \\ -0.0662 & -0.0662 & 0 & -0.0660 & 0 \\ -0.0301 & -0.0301 & 0 & 0.0005 & 0 \\ 0 & 0 & 0 & 0 & 0 \\ -0.0155 & 0.0155 & 0 & 0.0001 & 0.0349 \\ 0.0560 & -0.0560 & 0 & -0.0818 & 0.0349 \\ 0.0086 & -0.0086 & 0 & 0.0001 & -0.0170 \\ 0 & 0 & 0 & 0 & 0 \\ 0 & 0 & 0 & 0 & 0 \\ 0 & 0 & 0 & 0 & 0 \end{bmatrix}, \quad \boldsymbol{G}_{p1} = \begin{bmatrix} -0.0269 & 0.1010 & -0.0010 \\ -0.1624 & -0.5282 & -0.0023 \\ -0.0009 & 0.0068 & -0.0001 \\ 0 & 0 & 0 \\ 0 & 0 & -0.1518 \\ 0 & 0 & -0.1475 \\ 0 & 0 & 0.0246 \\ 0 & 0 & 0 \\ 0 & 0 & 0 \\ 0 & 0 & 1.0000 \end{bmatrix}$$

$$\boldsymbol{C}_{p1} = \begin{bmatrix} 0 & 0 & 0 & 0 & 0.6913 & 0 & 0 & 0 & 0 & 0 \\ 0.1396 & -0.9902 & 0 & 82.8800 & 0 & 0 & 0 & 0 & 0 & 0 \\ 0 & 0 & 0 & 0 & 0 & 0 & 0 & 0 & 0 & 1.0000 \end{bmatrix}$$

$$\boldsymbol{A}_{p2} = \begin{bmatrix} -0.0329 & 0.1816 & -19.2365 & -9.5191 & -0.0005 & 0 & 0 & 0 & 0 & 0 \\ -0.0737 & -0.6547 & 72.9036 & -2.3714 & -0.0028 & 0 & 0 & -0.0002 & 0 & 0 \\ 0.0045 & -0.0175 & -0.6891 & 0 & 0.0006 & 0 & -0.0029 & 0 & 0 & 0 \\ 0 & 0 & 1.0000 & 0 & 0 & 0 & 0 & 0 & 0 & 0 \\ 0 & 0 & 0 & 0 & -0.1419 & 20.1989 & -79.7753 & 9.5191 & 0 & 0 \\ 0 & 0 & 0.0003 & 0 & -0.1977 & -1.7046 & 0.9126 & 0 & 0 & 0 \\ 0 & 0 & 0.0025 & 0 & 0.0205 & -0.0474 & -0.2719 & 0 & 0 & 0 \\ 0 & 0 & 0 & 0 & 0 & 1.0000 & 0.2491 & 0 & 0 & 0 \\ 0 & 0 & 0 & 0 & 0 & 0 & 1.0306 & 0 & 0 & 0 \\ 0 & 0 & 0 & 0 & 1.0000 & 0 & 0 & -20.0352 & 82.8800 & 0 \end{bmatrix}$$

$$\boldsymbol{B}_{p2} = \begin{bmatrix} 0.0056 & 0.0056 & 0 & 0.0031 & 0 \\ -0.0696 & -0.0696 & 0 & -0.0716 & 0 \\ -0.0310 & -0.0310 & 0 & 0.0003 & 0 \\ 0 & 0 & 0 & 0 & 0 \\ -0.0157 & 0.0157 & 0 & -0.0028 & 0.0332 \\ 0.0580 & -0.0580 & 0 & -0.0871 & 0.0337 \\ 0.0084 & -0.0084 & 0 & -0.0011 & -0.0170 \\ 0 & 0 & 0 & 0 & 0 \\ 0 & 0 & 0 & 0 & 0 \\ 0 & 0 & 0 & 0 & 0 \end{bmatrix}, \quad \boldsymbol{G}_{p2} = \begin{bmatrix} -0.0329 & 0.1816 & -0.0005 \\ -0.0737 & -0.6547 & -0.0028 \\ 0.0045 & -0.0175 & 0.0006 \\ 0 & 0 & 0 \\ 0 & 0 & -0.1419 \\ 0 & 0 & -0.1977 \\ 0 & 0 & 0.0205 \\ 0 & 0 & 0 \\ 0 & 0 & 0 \\ 0 & 0 & 1.0000 \end{bmatrix}$$

$$\boldsymbol{C}_{p2} = \begin{bmatrix} 0 & 0 & 0 & 0 & 0.6913 & 0 & 0 & 0 & 0 & 0 \\ 0.2417 & -0.9703 & 0 & 82.8800 & 0 & 0 & 0 & 0.0004 & 0 & 0 \\ 0 & 0 & 0 & 0 & 0 & 0 & 0 & 0 & 0 & 1.0000 \end{bmatrix}$$

$$\boldsymbol{A}_{p3} = \begin{bmatrix} -0.0269 & 0.1010 & -10.9645 & -9.7139 & -0.0010 & 0 & 0 & 0 & 0 & 0 \\ -0.1624 & -0.5282 & 74.3778 & -1.3695 & -0.0023 & 0 & 0 & 0 & 0 & 0 \\ -0.0009 & 0.0068 & -0.6088 & 0 & -0.0001 & 0 & -0.0029 & 0 & 0 & 0 \\ 0 & 0 & 1.0000 & 0 & 0 & 0 & 0 & 0 & 0 & 0 \\ 0 & 0 & 0 & 0 & -0.1518 & 11.7055 & -81.4323 & 9.7139 & 0 & 0 \\ 0 & 0 & 0.0003 & 0 & -0.1475 & -1.7875 & 0.6768 & 0 & 0 & 0 \\ 0 & 0 & 0.0025 & 0 & 0.0246 & -0.0426 & -0.2379 & 0 & 0 & 0 \\ 0 & 0 & 0 & 0 & 0 & 1.0000 & 0.1410 & 0 & 0 & 0 \\ 0 & 0 & 0 & 0 & 0 & 0 & 1.0099 & 0 & 0 & 0 \\ 0 & 0 & 0 & 0 & 1.0000 & 0 & 0 & -11.5700 & 82.8800 & 0 \end{bmatrix}$$

$$\boldsymbol{B}_{p3} = \begin{bmatrix} 0.0135 & 0.0135 & -0.0066 & 0 & 0 \\ -0.0662 & -0.0662 & -0.0660 & 0 & 0 \\ -0.0301 & -0.0301 & 0.0005 & 0 & 0 \\ 0 & 0 & 0 & 0 & 0 \\ -0.0155 & 0.0155 & -0.0001 & 0 & 0.0349 \\ 0.0560 & -0.0560 & 0.0818 & 0 & 0.0349 \\ 0.0086 & -0.0086 & -0.0001 & 0 & -0.0170 \\ 0 & 0 & 0 & 0 & 0 \\ 0 & 0 & 0 & 0 & 0 \\ 0 & 0 & 0 & 0 & 0 \end{bmatrix}, \quad \boldsymbol{G}_{p3} = \begin{bmatrix} -0.0269 & 0.1010 & -0.0010 \\ -0.1624 & -0.5282 & -0.0023 \\ -0.0009 & 0.0068 & -0.0001 \\ 0 & 0 & 0 \\ 0 & 0 & -0.1518 \\ 0 & 0 & -0.1475 \\ 0 & 0 & 0.0246 \\ 0 & 0 & 0 \\ 0 & 0 & 0 \\ 0 & 0 & 1.0000 \end{bmatrix}$$

$$\boldsymbol{C}_{p3} = \begin{bmatrix} 0 & 0 & 0 & 0 & 0.6913 & 0 & 0 & 0 & 0 & 0 \\ 0.1396 & -0.9902 & 0 & 82.8800 & 0 & 0 & 0 & 0 & 0 & 0 \\ 0 & 0 & 0 & 0 & 0 & 0 & 0 & 0 & 0 & 1.0000 \end{bmatrix}$$

$$\boldsymbol{A}_{p4} = \begin{bmatrix} -0.0329 & 0.1816 & -19.2365 & -9.5191 & -0.0006 & 0 & 0 & 0 & 0 & 0 \\ -0.0737 & -0.6547 & 72.9036 & -2.3714 & -0.0028 & 0 & 0 & -0.0002 & 0 & 0 \\ 0.0045 & -0.0175 & -0.6891 & 0 & 0.0006 & 0 & -0.0029 & 0 & 0 & 0 \\ 0 & 0 & 1.0000 & 0 & 0 & 0 & 0 & 0 & 0 & 0 \\ 0 & 0 & 0 & 0 & -0.1419 & 20.1989 & -79.7753 & 9.5191 & 0 & 0 \\ 0 & 0 & 0.0003 & 0 & -0.1977 & -1.7046 & 0.9126 & 0 & 0 & 0 \\ 0 & 0 & 0.0025 & 0 & 0.0205 & -0.0474 & -0.2719 & 0 & 0 & 0 \\ 0 & 0 & 0 & 0 & 0 & 1.0000 & 0.2491 & 0 & 0 & 0 \\ 0 & 0 & 0 & 0 & 0 & 0 & 1.0306 & 0 & 0 & 0 \\ 0 & 0 & 0 & 0 & 1.0000 & 0 & 0 & -20.0352 & 82.8800 & 0 \end{bmatrix}$$

$$\boldsymbol{B}_{p4} = \begin{bmatrix} 0.0056 & 0.0056 & 0.0031 & 0 & 0 \\ -0.0696 & -0.0696 & -0.0716 & 0 & 0 \\ -0.0310 & -0.0310 & 0.0003 & 0 & 0 \\ 0 & 0 & 0 & 0 & 0 \\ -0.0157 & 0.0157 & 0.0028 & 0 & 0.0332 \\ 0.0580 & -0.0580 & 0.0871 & 0 & 0.0337 \\ 0.0084 & -0.0084 & 0.0011 & 0 & -0.0170 \\ 0 & 0 & 0 & 0 & 0 \\ 0 & 0 & 0 & 0 & 0 \\ 0 & 0 & 0 & 0 & 0 \end{bmatrix}, \quad \boldsymbol{G}_{p4} = \begin{bmatrix} -0.0329 & 0.1816 & -0.0006 \\ -0.0737 & -0.6547 & -0.0028 \\ 0.0045 & -0.0175 & 0.0006 \\ 0 & 0 & 0 \\ 0 & 0 & -0.1419 \\ 0 & 0 & -0.1977 \\ 0 & 0 & 0.0205 \\ 0 & 0 & 0 \\ 0 & 0 & 0 \\ 0 & 0 & 1.0000 \end{bmatrix}$$

$$\boldsymbol{C}_{p4} = \begin{bmatrix} 0 & 0 & 0 & 0 & 0.6913 & 0 & 0 & 0 & 0 & 0 \\ 0.2417 & -0.9703 & 0 & 82.8800 & 0 & 0 & 0 & 0.0004 & 0 & 0 \\ 0 & 0 & 0 & 0 & 0 & 0 & 0 & 0 & 0 & 1.0000 \end{bmatrix}$$

$$\boldsymbol{A}_{p5} = \begin{bmatrix} -0.0214 & 0.1311 & -15.1494 & -9.6280 & -0.0013 & 0 & 0 & 0 & 0 & 0 \\ -0.1165 & -0.6158 & 73.6492 & -1.8811 & -0.0040 & 0 & 0 & -0.0054 & 0 & 0 \\ 0.0002 & -0.0005 & -0.6472 & 0 & -0.0001 & 0 & -0.0029 & 0 & 0 & 0 \\ 0 & 0 & 1.0000 & 0 & 0 & 0 & -0.0006 & 0 & 0 & 0 \\ 0.0001 & -0.0010 & 0 & -0.0011 & -0.1472 & 16.0858 & -80.6884 & 9.6280 & 0 & 0 \\ -0.0007 & 0.0038 & 0.0003 & 0 & -0.1694 & -1.7556 & 0.8776 & 0 & 0 & 0 \\ -0.0001 & 0.0004 & 0.0025 & 0 & 0.0224 & -0.0482 & -0.2410 & 0 & 0 & 0 \\ 0 & 0 & 0.0001 & 0 & 0 & 1.0000 & 0.1954 & 0 & 0 & 0 \\ 0 & 0 & 0.0006 & 0 & 0 & 0 & 1.0189 & 0 & 0 & 0 \\ 0 & -0.0006 & 0 & 0 & 1.0000 & 0 & 0 & -15.8928 & 82.8800 & 0 \end{bmatrix}$$

$$\boldsymbol{B}_{p5} = \begin{bmatrix} 0 & 0.0074 & 0.0047 & -0.0067 & 0 \\ 0 & -0.0674 & -0.0760 & -0.0598 & 0 \\ 0 & -0.0302 & -0.0009 & 0.0018 & 0 \\ 0 & 0 & 0 & 0 & 0 \\ 0 & 0.0154 & 0.0016 & -0.0007 & 0.0336 \\ 0 & -0.0562 & 0.0937 & -0.0749 & 0.0340 \\ 0 & -0.0084 & 0.0021 & 0.0006 & -0.0169 \\ 0 & 0 & 0 & 0 & 0 \\ 0 & 0 & 0 & 0 & 0 \\ 0 & 0 & 0 & 0 & 0 \end{bmatrix}, \quad \boldsymbol{G}_{p5} = \begin{bmatrix} -0.0214 & 0.1311 & -0.0013 \\ -0.1165 & -0.6158 & -0.0040 \\ 0.0002 & -0.0005 & -0.0001 \\ 0 & 0 & 0 \\ 0.0001 & -0.0010 & -0.1472 \\ -0.0007 & 0.0038 & -0.1694 \\ -0.0001 & 0.0004 & 0.0224 \\ 0 & 0 & 0 \\ 0 & 0 & 0 \\ 0 & -0.0006 & 1.0000 \end{bmatrix}$$

$$\boldsymbol{C}_{p5} = \begin{bmatrix} 0 & 0 & 0 & 0 & 0.6913 & 0 & 0 & 0 & 0 & 0 \\ 0.1918 & -0.9814 & 0 & 82.8800 & -0.0006 & 0 & 0 & 0.0088 & 0 & 0 \\ 0 & 0 & 0 & 0 & 0 & 0 & 0 & 0 & 0 & 1.0000 \end{bmatrix}$$

$$\boldsymbol{A}_{p6} = \begin{bmatrix} -0.0214 & 0.1311 & -15.1425 & -9.6281 & -0.0011 & 0 & 0 & 0 & 0 & 0 \\ -0.1166 & -0.6158 & 73.6503 & -1.8803 & -0.0066 & 0 & 0 & 0.0052 & 0 & 0 \\ 0.0002 & -0.0005 & -0.6471 & 0 & -0.0002 & 0 & -0.0029 & 0 & 0 & 0 \\ 0 & 0 & 1.0000 & 0 & 0 & 0 & 0.0005 & 0 & 0 & 0 \\ -0.0001 & 0.0010 & 0 & 0.0010 & -0.1476 & 16.0789 & -80.6897 & 9.6281 & 0 & 0 \\ 0.0007 & -0.0037 & 0.0003 & 0 & -0.1679 & -1.7557 & 0.8775 & 0 & 0 & 0 \\ 0.0001 & -0.0004 & 0.0025 & 0 & 0.0223 & -0.0482 & -0.2410 & 0 & 0 & 0 \\ 0 & 0 & -0.0001 & 0 & 0 & 1.0000 & 0.1953 & 0 & 0 & 0 \\ 0 & 0 & -0.0006 & 0 & 0 & 0 & 1.0189 & 0 & 0 & 0 \\ 0 & 0.0005 & 0 & 0 & 1.0000 & 0 & 0 & -15.8858 & 82.8800 & 0 \end{bmatrix}$$

$$\boldsymbol{B}_{p6} = \begin{bmatrix} 0.0074 & 0 & -0.0067 & 0.0047 & 0 \\ -0.0674 & 0 & -0.0598 & -0.0760 & 0 \\ -0.0302 & 0 & 0.0018 & -0.0009 & 0 \\ 0 & 0 & 0 & 0 & 0 \\ -0.0154 & 0 & 0.0007 & -0.0016 & 0.0336 \\ 0.0562 & 0 & 0.0749 & -0.0937 & 0.0340 \\ 0.0084 & 0 & -0.0006 & -0.0021 & -0.0169 \\ 0 & 0 & 0 & 0 & 0 \\ 0 & 0 & 0 & 0 & 0 \\ 0 & 0 & 0 & 0 & 0 \end{bmatrix}, \quad \boldsymbol{G}_{p6} = \begin{bmatrix} -0.0214 & 0.1311 & -0.0011 \\ -0.1166 & -0.6158 & -0.0066 \\ 0.0002 & -0.0005 & -0.0002 \\ 0 & 0 & 0 \\ -0.0001 & 0.0010 & -0.1476 \\ 0.0007 & -0.0037 & -0.1679 \\ 0.0001 & -0.0004 & 0.0223 \\ 0 & 0 & 0 \\ 0 & 0 & 0 \\ 0 & 0.0005 & 1.0000 \end{bmatrix}$$

$$\boldsymbol{C}_{p6} = \begin{bmatrix} 0 & 0 & 0 & 0 & 0.6913 & 0 & 0 & 0 & 0 & 0 \\ 0.1917 & -0.9815 & 0 & 82.8800 & 0.0005 & 0 & 0 & -0.0085 & 0 & 0 \\ 0 & 0 & 0 & 0 & 0 & 0 & 0 & 0 & 0 & 1.0000 \end{bmatrix}$$

Acknowledgments

This work was supported jointly by DSO National Laboratories, Singapore, under Grant DSOCL-01144, and by Nanyang Technological University under Grant RGM34/01.

References

[1]Braff, R., Powell, J. D., and Dorfler, J., "Applications of GPS to Air Traffic Control," *Global Positioning System: Theory and Applications*, Vol. 2, Progress in Astronautics and Aeronautics, Vol. 164, AIAA, Reston, VA, 1996, pp. 327–374.

[2]Shue, S., and Agarwal, R. K., "Design of Automatic Landing Systems Using Mixed H_2/H_∞ Control," *Journal of Guidance, Control, and Dynamics*, Vol. 22, No. 1, 1999, pp. 103–114.

[3]Niewoehner, R. J., and Kaminer, I. I., "Design of an Autoland Controller for Carrier-Based F-14 Aircraft Using H_∞ Output-Feedback Synthesis," *Proceedings of the American Control Conference*, Inst. of Electrical and Electronics Engineers, edited by M. Peshkin, Vol. 3, 1994, pp. 2501–2505.

[4]Ochi, Y., and Kanai, K., "Automatic Approach and Landing for Propulsion Controlled Aircraft by H_∞ Control," *Proceedings of the 1999 IEEE International Conference on Control Applications*, Inst. of Electrical and Electronics Engineers, Vol. 2, 1999, pp. 997–1002.

[5]Miller, W. T., Sutton, R. S., and Werbos, P. J., *Neural Networks for Control*, Bradford Book, MIT Press, Cambridge, MA, 1992, pp. 403–426.

[6]Saini, G., and Balakrishnan, S. N., "Adaptive Critic Based Neurocontroller for Autolanding of Aircraft," *Proceedings of the American Control Conference*, Inst. of Electrical and Electronics Engineers, Vol. 2, 1997, pp. 1081–1085.

[7]Che, J., and Chen, D. G., "Automatic Landing Control Using H_∞ Control and Stable Inversion," *Proceedings of the 40th IEEE Conference on Decision and Control*, Inst. of Electrical and Electronics Engineers, Vol. 1, 2001, pp. 241–246.

[8]Liao, F., Wang, J. L., and Yang, G. H., "Reliable Robust Flight Tracking Control: An LMI Approach," *IEEE Transactions on Control Systems Technology*, Vol. 10, No. 1, 2002, pp. 76–89.

[9]Veillette, R. J., Medanić, J. V., and Perkins, W. R., "Design of Reliable Control Systems," *IEEE Transactions on Automatic Control*, Vol. 37, No. 3, 1992, pp. 290–304.

[10]Tao, G., Chen, S., Tang, X. D., and Joshi, S. M., "An Adaptive Control Scheme for Systems with Unknown Actuator Failures," *Automatica*, Vol. 38, No. 6, 2002, pp. 1027–1034.

[11]Tao, G., Chen, S., Tang, X. D., and Joshi, S. M., *Adaptive Control of Systems with Actuator Failures*, Springer-Verlag, New York, 2004.

[12]Yang, G. H., and Lum, K. Y., "Fault-Tolerant Flight Tracking Control with Stuck Faults," *Proceedings of the American Control Conference*, Inst. of Electrical and Electronics Engineers, Vol. 1, 2003, pp. 521–526.

[13]Zhao, Q., and Jiang, J., "Reliable State-Feedback Control Systems Design Against Actuator Failures," *Automatica*, Vol. 30, No. 10, 1998, pp. 1267–1272.

[14]Nguyen, L. T., Ogburn, M. E., Gilbert, W. P., Kibler, K. S., Brown, P. W., and Deal, P. L., "Simulator Study of Stall/Post-Stall Characteristics of a Fighter Airplane with Relaxed Longitudinal Static Stability," NASA TP 1538, 1979.

[15]Teo, S. G., "Autolanding System Study: Aerodynamic Data of an Aircraft with Independent Control Surfaces by CFD," DSO National Lab., Technical Rept., Singapore, 2003.

[16]Scharfenberg, K. A., "Polarimetric Radar Observations of a Microburst-Producing Thunderstorm During Landing," *IEEE Transactions on Neural Network*, Vol. 9, No. 2, 1998, pp. 308–318.

[17]Zhou, K. M., and Doyle, J. C., *Essentials of Robust Control*, Prentice–Hall, Upper Saddle River, NJ, 1998.

[18]Khargonekar, P. P., Petersen, I. R., and Zhou, K., "Robust Stabilization of Uncertain Linear Systems: Quadratic Stability and H_∞ Control Theory," *IEEE Transactions on Automatic Control*, Vol. 35, No. 3, 1990, pp. 356–361.

[19]Apkarian, P., Tuan, H. D., and Bernussou, J., "Continuous-Time Analysis, Eigenstructure Assignment, and H_2 Synthesis with Enhanced Linear Matrix Inequalities (LMI) Characterizations," *IEEE Transactions on Automatic Control*, Vol. 46, No. 12, 2001, pp. 1941–1946.

[20]Gahinet, P., Nemirovski, A., Laub, A. J., and Chilali, M., *LMI Control Toolbox*, MathWorks, Inc., Natick, MA, 1995.